UNIVERSITÀ DEGLI STUDI DI SALERNO

DIPARTIMENTO DI FISICA "E. R. CAIANIELLO"

DOCTOR OF PHILOSOPHY IN PHYSICS

XIV CICLO, II SERIE

INTERFACE EFFECTS IN SUPERCONDUCTING HETEROSTRUCTURES

MARILENA CATAPANO

SUPERVISOR
PROF. ROBERTA CITRO

COORDINATOR
PROF. CANIO NOCE

2014 - 2015

There are no failures,
but only unsuccessful
attempts.

To my family.

Abstract

This work debates a theoretical investigation of the interfacial effects about heterostructures with normal metals and superconductors. At the beginning we will introduce the basic physical phenomena our calculations deal with and will describe a few experimental results. Then we will provide a description of the Blonder-Tinkham and Klapwijk (BTK) model for normal metal/superconductor junctions and we will introduce the attempt to generalize it to include proximity effect. After we will describe a generalized BTK model introducing a particle-hole mixing interface potential and we will present the main results. Finally, we will extend BTK model to include a spin-dependent potential, e.g. Rashba spin-orbit coupling, at the interface and we will analyze the spin transport properties.

Contents

Introduction

The interplay between the different properties of materials constituting heterostructures has an important influence on the complicated details of interfaces. The identification of interface effects in heterostructures has been in the focus of experimental and theoretical investigation. Theoretical work describes and predicts numerous manifestations of the influence between different long-range orderings[1, 2, 3, 46]. These effects appear due to the different nature of the decay of the superconducting correlations in the materials that are proximity coupled with a superconductor. In the case of a normal metal/superconductor (N/S) bilayer the superconducting transition temperature, T_c, decreases exponentially with characteristic length ξ_N, as the thickness of the overlaying N layer increases. This is understood as an effect caused by leakage of the superconducting pairs from S into N layer. On the other hand, any proximity of a ferromagnet (F) with a superconductor has been found to be detrimental to superconductivity. This has been understood as a pair-breaking effect of the magnetic moment when the superconducting pairs enter the F layer. Several theories has been developed to explain the proximity effect in F/S bilayer, predicting the oscillatory T_c behavior as a function of the thickness of F layer. Thus understanding the role of the potentials at the interface of superconducting structures is of primary importance. With the advent of the point contact spectroscopy, the study of several phenomena at the interface between a superconductor and non-superconducting materials have become accessible, but many questions remain open. In fact, the quality of the interface determines the transmission and reflection probabilities near the interface, that depend on the energy and spin of the incoming electron, and strongly influences the transport. From the theoretical point of view, the Blonder-Tinkham-Klapwijk (BTK) theory[32] provides a theoretical model for the interpretation of the current - voltage characteristic obtained through the point contact spectroscopy. The theory, based on the Bogoliubov-de Gennes (BdG) equations, permits to obtain the transmission and reflection probabilities in N/S junctions. By modelling the barrier potential at the interface by a Dirac delta potential of arbitrary am-

plitude, they are able to describe the current-voltage curves ranging from the tunnel junction to the metallic limit. Using the results of the BTK theory, a good agreement between theory and experiments was observed. However, in some cases, as in Cu/Nb junctions, the conductance shows particular structures which are not reproduced in BTK formalism. In particular, there appear two dips[21, 49, 50, 4, 5, 34, 6, 33] below but close to the superconducting energy gap. An attempt to explain such anomalies has been based on a proximity model[33] where the inclusion of the proximity effect is explained in terms of the existence of two energy gaps: the proximity gap and the bulk gap. Neverthless, such a theory is not the possible scenario and the aim of the present work is to describe the conductance features in a more general context, that of generalized boundary conditions in the BdG scattering problem. The proposed boundary conditions include a non-diagonal contribution in the particle-hole representation whose physical meaning is related to the proximity effects induced by the bulk superconductor on the normal side of the interface. Finally, we consider the effect of a spin-orbit interaction at the interface and try to characterize the spin current and the spin differential conductance.

This work is organized as follows. In Chapter 1 we introduce the basic physical phenomena of superconductivity and the Bogoliubov-de Gennes equations along with the description of few experimental results on charge transport. In Chapter 2 we provide a detailed description of the Blonder, Tinkham and Klapwijk (BTK) theory and we introduce the previous attempt to generalize it to include proximity effect. In Chapter 3 we describe a generalized BTK theory introducing a particle-hole mixing interface potential, which consists in imposing non-diagonal boundary conditions on the wave functions that describe the scattering processes at the interface and we will present the main results. In Chapter 4 we generalize BTK theory to include Rashba spin-orbit at the interface and we will analyze the spin transport properties in in normal metal/superconductor junctions. Finally, we give conclusions and outlook.

Chapter 1

Preliminaries and Motivation

In this chapter we briefly review the different regimes of electron transport in heterostructures and then focus on superconductivity. Starting from the Bardeen-Cooper-Schrieffer (BCS) theory, we introduce the mathematical formulation based on the Bogoliubov de Gennes (BdG) equations. Then we focus on a particular experimental probe of quasiparticles transport in superconducting junctions, the point contact Andreev reflection (PCAR) spectroscopy.

1.1 Electron transport in heterostructures: different regimes

The transport in heterostructures is determined by several characteristic length scales. The first is the Fermi wavelength, $\lambda_F = 2\pi/k_F$, which characterizes the electron wavelength itself at the Fermi energy for the transport. This important quantity depends on the total electron number. The second is the mean free path, $l_e = v_F\tau$, which characterizes the average length that an electron travels without scattering with other impurities. Here v_F is the Fermi velocity and the relaxation time τ is the elastic scattering time for electron transport. For an electron density $n_s = 5 \times 10^{11}/cm^2$ the Fermi wavelength is about $35nm$, while the mean free path is of $30\mu m$, with $v_F = 3 \times 10^7 cm/s$ and $\tau = 100ps$[7]. The third is the phase coherence length, L_ϕ, which characterizes the length that an electron wave packet can travel without losing its phase coherence. L_ϕ has a strong dependence on temperature, increasing as the temperature decreases, and might be larger than the mean free path l_e in *low-temperature* regime[8, 9, 10]. At low temperatures L_ϕ is about of a few micrometers. Comparing mean free path with characteristic dimensions of the system along one spatial dimension, L,

one can discriminate between different regimes of transport: *diffusive* regime $L \gg l_e$ and *ballistic* regime $L \ll l_e$, of interest here. Such a classification appears incomplete in the situation where different dimensions of the sample are substantially different. Mesoscopic systems with $L \sim l_e$ are definite to be in the *intermediate* regime. For a ballistic system $L_\phi = v_F \tau_\phi$ with τ_ϕ the phase-relaxation time that describes relaxation of the phase memory, while in diffusive conductors $L_\phi = \sqrt{D\tau_\phi}$ with $D = v_F l_e/d$ being the diffusion coefficient and d the dimensionality of the system. Another characteristic length is the thermal length also called Thouless length, $L_T = (\hbar D/k_B T)^{1/2}$, with k_B the Boltzmann constant and T the temperature, which describes dephasing of the electrons due to the thermal excitation in the system. If $L_T > L_\phi$ the thermal effects are minimal, while if $L_T < L_\phi$ the thermal effects cause dephasing of the electrons in the system. L_T and L_ϕ provide the temperature dependence of mesoscopic phenomena[11].

1.2 Superconductivity

Superconductors are materials that, below a critical temperature T_c, exhibit zero electrical resistance and perfect diamagnetism. The microscopic interpretation of a superconductor was provided by J. Bardeen, L. N. Cooper and R. Schrieffer (BCS)[14] in the famous BCS theory, that employs the Fröhlich Hamiltonian[12] of the electron-phonon interaction. An electron moving in a crystal lattice attracts the positive ions displacing them from the lattice and increasing the positive charge density due to the ions. The positively charged area in the lattice has an attractive effect on another electron. The lattice deformation therefore causes a weak attraction between pairs of electrons (Cooper pair). The BCS theory bases on the assumption that superconductivity arises when the attractive Cooper pair [13] interaction dominates over the repulsive Coulomb interaction. A Cooper pair is formed by two electrons due to exchange of a phonon. In general, Cooper pairs can be in a state of either total spin $S = 0$ (spin singlet) or $S = 1$ (spin triplet). To respect the antisymmetry under exchange of particles, the antysymmetric spin singlet state is accompaneid by a symmetric orbital wave function (even parity) with orbital angular momentum $L = 0$ $(s-wave)$, $L = 2$ $(d-wave)$, etc. The symmetric spin triplet state is accompanied by an antysymmetric orbital wave function (odd parity) with orbital angular momentum $L = 1$ $(p-wave)$, $L = 3$ $(f-wave)$, etc. In the BCS theory, Cooper pair is a two electron bound state with zero total momentum and spin $(\mathbf{k}\uparrow, -\mathbf{k}\downarrow)$. The typical distance between the two electrons that can form a pair is called *coherence length* and is given by $\xi = \hbar v_F/\pi\Delta$, where v_F is the Fermi velocity

and Δ is the energy gap that represents the minimum energy per electron needed to break one of the Cooper pair and is the central parameter in the BCS theory. In conventional superconductor ($s-wave$ Cooper pairs) typical values of ξ are of the order of thousand Å. At $T=0$ in the superconducting ground state electrons are involved only as pairs and the superconducting ground state takes the following form $|\psi_{BCS}\rangle = \prod_{\mathbf{k}} \left(u_{\mathbf{k}} + v_{\mathbf{k}} c^{\dagger}_{\mathbf{k}\uparrow} c^{\dagger}_{-\mathbf{k}\downarrow}\right)|0\rangle$ under the constraint $|u_{\mathbf{k}}|^2 + |v_{\mathbf{k}}|^2 = 1$, where $|0\rangle$ is the vacuum state, $u_{\mathbf{k}}$ and $v_{\mathbf{k}}$ represent the probability amplitudes that the pair $(\mathbf{k}\uparrow, -\mathbf{k}\downarrow)$ is unoccupied and occupied, respectively. Since the Cooper pairs are bosons, all of them occupy the same state of lowest energy and are separated by the energy gap 2Δ from a higher single levels into which normal electrons can be excited (*see* Fig. 1.1). The value of this gap is at zero temperature $\Delta_0 = 1.76 k_B T_c$. This approximation is valid in the weak coupling limit, which means superconductors for which $N(E_F)V \ll 1$ with $N(E_F)$ is the normal metal density of states at the Fermi energy and V the attractive interaction[15, 16, 17]. At

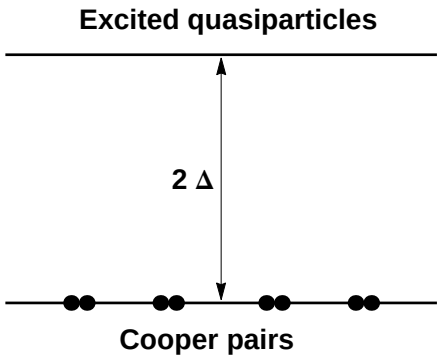

Figure 1.1: Energy levels diagram for a superconductor.

finite temperature some electrons can be thermally excited across the gap. This reduce the number of Cooper pairs and form the so-called quasiparticles that are coherent mixtures of particles and holes. These mixed particle-hole excited states are known as *Bogolons*. Therefore, with increasing the temperature, the energy gap decreases until near the critical temperature vanishes according to the law $\Delta(T)/\Delta_0 = 1.74\,(1 - T/T_c)^{1/2}$. For conventional superconductors experimental measurements of the energy gap are in good agreement with the BCS theory predictions[18]. Despite the brilliant success of the BCS theory, that provides a complete understanding of conventional

superconductors, it is applicable only to cases of weak coupling between the electron and the phonon and for translational invariant systems. In presence of arbitrary external potential $U(\mathbf{r})$, that can describe the effects of impurities and of the specimen surface, or a magnetic field $\mathbf{H}$, the Bogoliubov-de Gennes equations are a more powerful method to describe superconductivity. They can also describe non superconducting materials, such as a normal metal (N) or a ferromagnet (F), therefore can be used for any heterostructure.

1.3 Bogoliubov de Gennes equations

The Bogoliubov-de Gennes (BdG) equations[19] generalize the BCS formalism to treat spatially non-uniform superconductors. The real-space Hamiltonian written in terms of field operators $\psi_\sigma(\mathbf{r})$, $\psi_\sigma^\dagger(\mathbf{r})$ reads

$$\begin{aligned}\mathcal{H} &= \sum_\sigma \int d\mathbf{r}\psi_\sigma^\dagger(\mathbf{r})\,\mathcal{H}_0(\mathbf{r})\,\psi_\sigma(\mathbf{r}) \\ &- \frac{V}{2}\sum_{\sigma,\sigma'}\int d\mathbf{r}\psi_\sigma^\dagger(\mathbf{r})\,\psi_{\sigma'}^\dagger(\mathbf{r})\,\psi_{\sigma'}(\mathbf{r})\,\psi_\sigma(\mathbf{r}),\end{aligned} \tag{1.1}$$

where $\mathcal{H}_0(\mathbf{r})$ is the single-particle Hamiltonian given by

$$\mathcal{H}_0(\mathbf{r}) = \left[\frac{1}{2m}\left(-i\hbar\nabla - e\mathbf{A}(\mathbf{r})\right)^2 + U(\mathbf{r}) - \mu\right], \tag{1.2}$$

with $\mathbf{A}(\mathbf{r})$ the vector potential, $U(\mathbf{r})$ the external spin-indipendent potential that includes the boundary and static impurity potentials and μ is the chemical potential, σ is the spin index and V is the attractive interaction responsible for superconductivity assumed to be constant (BCS approximation). In presence of a spin-dependent potential, such as Zeeman or spin-orbit coupling terms, to the Hamiltonian in Eq. (1.1) is added the following term:

$$\mathcal{H}_m = \sum_{\sigma,\sigma'}\int d\mathbf{r}\psi_\sigma^\dagger(\mathbf{r})\,U_{\sigma\sigma'}(\mathbf{r})\,\psi_{\sigma'}(\mathbf{r}), \tag{1.3}$$

where $U_{\sigma\sigma'}(\mathbf{r})$ is a matrix proportional to a Pauli matrix. Therefore the total Hamiltonian becomes

$$\begin{aligned}\mathscr{H} &= \sum_\sigma \int d\mathbf{r}\psi_\sigma^\dagger(\mathbf{r})\,\mathcal{H}_0(\mathbf{r})\,\psi_\sigma(\mathbf{r}) + \sum_{\sigma,\sigma'}\int d\mathbf{r}\psi_\sigma^\dagger(\mathbf{r})\,U_{\sigma\sigma'}(\mathbf{r})\,\psi_{\sigma'}(\mathbf{r}) \\ &- \frac{V}{2}\sum_{\sigma,\sigma'}\int d\mathbf{r}\psi_\sigma^\dagger(\mathbf{r})\,\psi_{\sigma'}^\dagger(\mathbf{r})\,\psi_{\sigma'}(\mathbf{r})\,\psi_\sigma(\mathbf{r}).\end{aligned} \tag{1.4}$$

The annihilation and the creation field operators $\psi_\sigma(\mathbf{r})$ and $\psi_\sigma^\dagger(\mathbf{r})$ satisfy ordinary fermion anticommutations relations

$$\begin{aligned} \left\{\psi_\sigma(\mathbf{r}), \psi_{\sigma'}^\dagger(\mathbf{r}')\right\} &= \delta(\mathbf{r}-\mathbf{r}')\,\delta_{\sigma\sigma'} \\ \{\psi_\sigma(\mathbf{r}), \psi_{\sigma'}(\mathbf{r}')\} &= \left\{\psi_\sigma^\dagger(\mathbf{r}), \psi_{\sigma'}^\dagger(\mathbf{r}')\right\} = 0, \end{aligned} \tag{1.5}$$

where $\delta(\mathbf{r})$ is the Dirac delta function and δ_{ab} is the Kronecker delta symbol. Making a mean-field treatment of the interaction term (second term in Eq. (1.4))

$$\begin{aligned} &\psi_\sigma^\dagger(\mathbf{r})\,\psi_{\sigma'}^\dagger(\mathbf{r})\,\psi_{\sigma'}(\mathbf{r})\,\psi_\sigma(\mathbf{r}) \approx \langle\psi_\sigma^\dagger(\mathbf{r})\,\psi_{\sigma'}^\dagger(\mathbf{r})\rangle\psi_{\sigma'}(\mathbf{r})\,\psi_\sigma(\mathbf{r}) \\ &+\psi_\sigma^\dagger(\mathbf{r})\,\psi_{\sigma'}^\dagger(\mathbf{r})\,\langle\psi_{\sigma'}(\mathbf{r})\,\psi_\sigma(\mathbf{r})\rangle - \underbrace{\langle\psi_\sigma^\dagger(\mathbf{r})\,\psi_{\sigma'}^\dagger(\mathbf{r})\rangle\langle\psi_{\sigma'}(\mathbf{r})\,\psi_\sigma(\mathbf{r})\rangle}_{constant}, \end{aligned} \tag{1.6}$$

defining the pairing potential as $\Delta_{\sigma\sigma'}(\mathbf{r}) = -V\langle\psi_{\sigma'}(\mathbf{r})\,\psi_\sigma(\mathbf{r})\rangle$ and omitting the constant term, the Hamiltonian (Eq. (1.4)) becomes

$$\begin{aligned} \mathscr{H}_{eff} &= \sum_\sigma \int d\mathbf{r}\psi_\sigma^\dagger(\mathbf{r})\,\mathcal{H}_0(\mathbf{r})\,\psi_\sigma(\mathbf{r}) + \sum_{\sigma,\sigma'}\int d\mathbf{r}\psi_\sigma^\dagger(\mathbf{r})\,U_{\sigma\sigma'}(\mathbf{r})\,\psi_{\sigma'}(\mathbf{r}) \\ &+ \sum_{\sigma,\sigma'}\int d\mathbf{r}\left[\Delta_{\sigma\sigma'}^\dagger(\mathbf{r})\,\psi_{\sigma'}(\mathbf{r})\,\psi_\sigma(\mathbf{r}) + \Delta_{\sigma\sigma'}(\mathbf{r})\,\psi_\sigma^\dagger(\mathbf{r})\,\psi_{\sigma'}^\dagger(\mathbf{r})\right], \end{aligned} \tag{1.7}$$

where for an s-wave superconductor $\Delta_{\sigma\sigma'}(\mathbf{r}) = (i\hat{\sigma}_y)_{\sigma\sigma'}\Delta(\mathbf{r})$ with $\hat{\sigma}_y$ the Pauli matrix. This Hamiltonian has a bilinear form in $\psi_\sigma(\mathbf{r})$ and $\psi_\sigma^\dagger(\mathbf{r})$ operators and may be diagonalized by the following canonical transformations introduced by Bogoliubov

$$\psi_\sigma(\mathbf{r}) = \sum_n \left[u_{n\sigma}(\mathbf{r})\,\gamma_n + v_{n\sigma}^*(\mathbf{r})\,\gamma_n^\dagger\right], \tag{1.8}$$

where the operators $\gamma_n^\dagger$ and γ_n that, creates and annihilates a quasiparticle in the state n, respectively, satisfy ordinary fermion anticommutation relations

$$\begin{aligned} \{\gamma_n, \gamma_{n'}^\dagger\} &= \delta_{nn'} \\ \{\gamma_n, \gamma_{n'}\} &= \{\gamma_n^\dagger, \gamma_{n'}^\dagger\} = 0. \end{aligned} \tag{1.9}$$

The transformation yields the following diagonal form of the Hamiltonian (Eq. (1.7))

$$\mathscr{H}_{eff} = E_0 + \sum_n E_n\gamma_n^\dagger\gamma_n, \tag{1.10}$$

where E_0 is the ground state energy and E_n is the energy of the excitation n. Furthermore, we have

$$\begin{aligned} \left[\mathscr{H}_{eff}, \gamma_n^\dagger\right] &= E_n \gamma_n^\dagger \\ \left[\mathscr{H}_{eff}, \gamma_n\right] &= -E_n \gamma_n. \end{aligned} \tag{1.11}$$

In order to derive the equations for $u_{n\sigma}(\mathbf{r})$ and $v_{n\sigma}(\mathbf{r})$ contained in the Eq. (1.8) we calculate the commutator $[\psi_\sigma(\mathbf{r}), \mathscr{H}_{eff}]$ using Eq. (1.7) and the anticommutation properties of the operators $\psi_\sigma^\dagger(\mathbf{r})$ and $\psi_\sigma(\mathbf{r})$, obtaining

$$\left[\psi_\sigma(\mathbf{r}), \mathscr{H}_{eff}\right] = \mathcal{H}_0 \psi_\sigma(\mathbf{r}) + \sum_{\sigma'} U_{\sigma\sigma'}(\mathbf{r}) \psi_{\sigma'}(\mathbf{r}) + \sum_{\sigma'} \Delta_{\sigma\sigma'}(\mathbf{r}) \psi_{\sigma'}^\dagger(\mathbf{r}). \tag{1.12}$$

Applying the Bogoliubov transformation given by Eq. (1.8), employing the anticommutation rules of the operators γ_n and $\gamma_n^\dagger$ and taking into account the commutators in Eq. (1.11) we have

$$\begin{aligned} \sum_n E_n u_{n\sigma}(\mathbf{r}) \gamma_n &- \sum_n E_n v_{n\sigma}^*(\mathbf{r}) \gamma_n^\dagger = \sum_n \mathcal{H}_0(\mathbf{r}) u_{n\sigma}(\mathbf{r}) \gamma_n \\ &+ \sum_n \mathcal{H}_0(\mathbf{r}) v_{n\sigma}^*(\mathbf{r}) \gamma_n^\dagger + \sum_{n\sigma'} U_{\sigma\sigma'}(\mathbf{r}) u_{n\sigma'}(\mathbf{r}) \gamma_n \\ &+ \sum_{n\sigma'} U_{\sigma\sigma'}(\mathbf{r}) v_{n\sigma'}^*(\mathbf{r}) \gamma_n^\dagger + \sum_{n\sigma'} \Delta_{\sigma\sigma'} v_{n\sigma'}(\mathbf{r}) \gamma_n \\ &+ \sum_{n\sigma'} \Delta_{\sigma\sigma'} u_{n\sigma'}^*(\mathbf{r}) \gamma_n^\dagger. \end{aligned} \tag{1.13}$$

Comparing the coefficients of γ_n and $\gamma_n^\dagger$ on the two sides of the equation, we obtain:

$$\begin{aligned} E_n u_{n\sigma}(\mathbf{r}) &= \mathcal{H}_0(\mathbf{r}) u_{n\sigma}(\mathbf{r}) + \sum_{\sigma'} U_{\sigma\sigma'}(\mathbf{r}) u_{n\sigma'}(\mathbf{r}) + \sum_{\sigma'} \Delta_{\sigma\sigma'} v_{n\sigma'}(\mathbf{r}) \\ -E_n v_{n\sigma}(\mathbf{r}) &= \mathcal{H}_0^*(\mathbf{r}) v_{n\sigma}(\mathbf{r}) + \sum_{\sigma'} U_{\sigma\sigma'}^*(\mathbf{r}) v_{n\sigma'}(\mathbf{r}) + \sum_{\sigma'} \Delta_{\sigma\sigma'}^*(\mathbf{r}) u_{n\sigma'}(\mathbf{r}), \end{aligned} \tag{1.14}$$

that are called *Bogoliubov-de Gennes (BdG) equations*, where we have conjugated both sides of the second equation. The equations can be written in a matrix form, using the four-component Nambu spinor $\psi_n(\mathbf{r}) = (u_{n\uparrow}(\mathbf{r}), u_{n\downarrow}(\mathbf{r}), v_{n\uparrow}(\mathbf{r}), v_{n\downarrow}(\mathbf{r}))^t$, as

$$\begin{pmatrix} \mathcal{H}_1(\mathbf{r}) & U_{\uparrow\downarrow}(\mathbf{r}) & 0 & \Delta(\mathbf{r}) \\ U_{\downarrow\uparrow}(\mathbf{r}) & \mathcal{H}_2(\mathbf{r}) & -\Delta(\mathbf{r}) & 0 \\ 0 & -\Delta^*(\mathbf{r}) & -\mathcal{H}_1^*(\mathbf{r}) & -U_{\uparrow\downarrow}^*(\mathbf{r}) \\ \Delta^*(\mathbf{r}) & 0 & -U_{\downarrow\uparrow}^*(\mathbf{r}) & -\mathcal{H}_2^*(\mathbf{r}) \end{pmatrix} \begin{pmatrix} u_\uparrow(\mathbf{r}) \\ u_\downarrow(\mathbf{r}) \\ v_\uparrow(\mathbf{r}) \\ v_\downarrow(\mathbf{r}) \end{pmatrix} = E \begin{pmatrix} u_\uparrow(\mathbf{r}) \\ u_\downarrow(\mathbf{r}) \\ v_\uparrow(\mathbf{r}) \\ v_\downarrow(\mathbf{r}) \end{pmatrix}. \tag{1.15}$$

where $\mathcal{H}_1(\mathbf{r}) = \mathcal{H}_0(\mathbf{r}) + U_{\uparrow\uparrow}(\mathbf{r})$ and $\mathcal{H}_2(\mathbf{r}) = \mathcal{H}_0(\mathbf{r}) + U_{\downarrow\downarrow}(\mathbf{r})$ and the index n of the excitation has been omitted. The Bogoliubov-de Gennes equations allow to get the states of the system both in superconducting and non-superconducting materials. In the absence of spin-flip scattering, the four-component BdG equations may be decoupled into two sets of two-component equations: one for spin-up electron-like and spin-down hole-like quasiparticle wave functions $(u_\uparrow(\mathbf{r}), v_\downarrow(\mathbf{r}))$, the other for $(u_\downarrow(\mathbf{r}), v_\uparrow(\mathbf{r}))$.

1.4 Andreev reflection

Andreev reflection[23] is the fundamental process inducing the proximity effect and hence all phenomena related to it [24, 25, 26]. The proximity effect is the occurence of superconducting-like properties in non-superconducting materials placed in contact with a superconductor (S). In other words, Cooper pairs from a superconducting metal in close proximity can diffuse into the normal metal, making a normal metal (N) layer weakly superconductive[27]. The thickness of this superconductive region on the normal side exceeds the superconducting coherence length and depends on different parameters, such as temperature, presence of impurities, tunnel barrier or boundaries. At first sight, this proximity effect does not seem possible since no attactive electron interaction exists in the normal region and thus no superconducting correlations can be created. However, these correlations can leak from superconductor into the normal region by means of Andreev reflection[28]. Due to the existence of an energy gap at the Fermi energy in the density of states of the superconductor, an incoming electron can be transmitted into it according to two different mechanisms depending on its energy. An incoming electron with energy larger than the superconducting energy gap can freely propagate into the superconductor, where it will be converted into a quasiparticle with the same energy. Since there are no accessible single particle states for energy lower than the superconducting energy gap, the only possibility for an incoming electron to be transmitted into the superconductor is by forming a Cooper pair (*see* Fig. 1.2). In order to do that, it must couple with another electron from the normal metal with opposite wave vector and spin. This process is equivalent to the reflection of a hole. A total charge $2e$ is transmitted from the normal metal to the superconductor [29]. As a consequence, the Andreev reflection allows a conversion of the dissipative electrical current in the normal metal into a dissipationless supercurrent. When a ferromagnet/superconductor (F/S) junction is considered the situation is strongly modified because the incoming electron and the Andreev reflected hole occupy opposite spin bands and in a ferromagnet

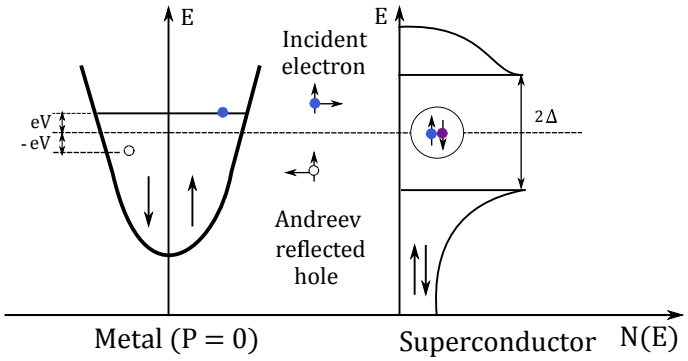

Figure 1.2: Andreev reflection process for a metal with spin polarization of $P = 0$. The solid circles denote electrons and open circles denote holes.

the spin-up and the spin-down band are different (*see* Fig. 1.3). An imme-

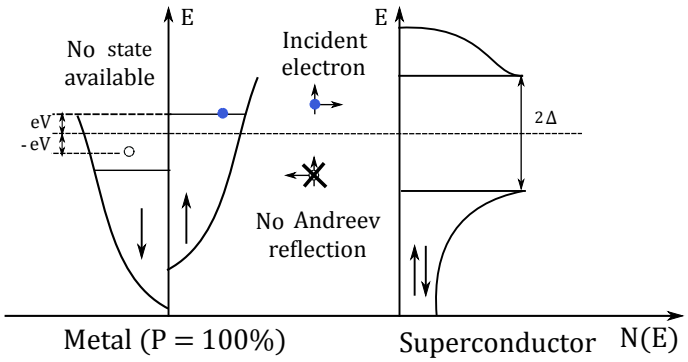

Figure 1.3: Andreev reflection process for a metal with spin polarization of $P = 100\%$. The solid circles denote electrons and open circles denote holes.

diate consequence is the total suppression of Andreev reflection in a fully spin-polarized metal [30]. This effect can be used to measure the spin polarization of metals using direct differential conductance measurements through the point contact Andreev reflection spectroscopy.

1.4.1 Point contact Andreev reflection spectroscopy

Point contact Andreev reflection (PCAR) is a technique introduced by Soulen *et al.* [21] and Upadhyay *et al.*[22], based on Andreev reflection (AR), where a narrow superconducting tip, e.g. *Nb*, is placed into contact with a normal conductor at temperatures below the critical temperature of the tip. When a bias voltage across the tip/sample junction is applied the differential conductance is measured. Andreev reflection is studied from the analysis of the

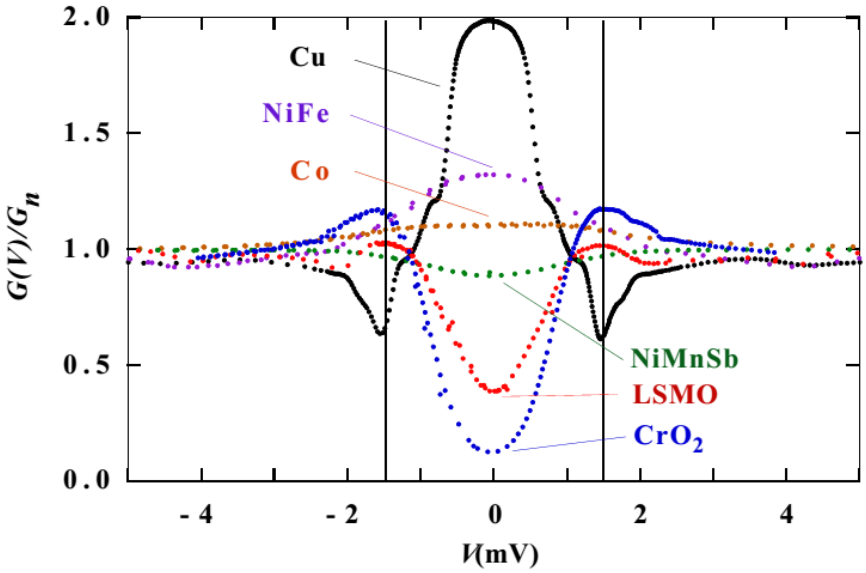

Figure 1.4: The differential conductance for several spin-polarized metals showing the suppression of Andreev reflection with increasing spin polarization. Figure adapted from Ref.[21].

normalized differential conductance $G(V)/G_N$ *vs* V, where $G(V) = dI/dV$, $G_N = G(eV \gg \Delta)$ and V is the bias voltage, known as PCAR spectrum. PCAR spectrum is analyzed within the standard Blonder-Tinkham-Klapwijk (BTK) theory[32](will be discuss more thoroughly in the next chapter). The theory, formulated in terms of BdG equations, provides the transmission and reflection coefficients of a N/S junction and allows to get, introducing a tunneling barrier, the characteristic differential conductance, ranging from metallic (zero tunneling barrier) to the tunneling regime (high tunneling barrier). Using this approach they were able to obtain an accurate prediction of properties such as the energy gap, the excess current due to the Andreev reflection and an explanation of the conversion of a quasiparticle current into supercurrent. When we have a normal metal coupled to a superconductor the differential conductance below the gap is just twice the normal state conductance G_N of the junction. In a ferromagnet the Andreev reflection is suppressed due to the unequal density of states of up and down spins and the PCAR spectra are analyzed within a modified BTK theory to include the spin polarization[21, 22, 31]. In PCAR spectrum two characteristic values are commonly discussed: the conductance at zero bias voltage, that reflects the degree of Andreev reflection in the point contact, and the conductance near $e|V| = \Delta$, which is named Δ conductance peak. In Fig. 1.4 is exhib-

ited the normalized differential conductance for different metals, with Nb as superconducting material, showing the suppression of $G(V)/G_n$ at zero bias voltage with increasing spin polarization, due to the suppression of Andreev reflection. Indeed, depending on the material the differential conductance range varies from 2 to almost zero. For Cu/Nb contact the differential conductance shows sharp dips, at the postition of the Nb superconducting gap (the vertical lines in Fig. 1.4), that are not expected in the BTK formalism. Many possible explanations[33, 34, 35] have been proposed for these dips, but the origin of their appearance is still under debate. In the following of this work we will introduce a general class of boundary conditions within the BTK theory which lead to a good description of the peak-dips structure in the conductance observed in some PCAR spectra. Singling out the microscopic models that describe the interface effects in superconducting heterostructures that pertain the interface properties and the bulk effects and that successfully describe the PCAR experimental outcomes represents the main objective of this work.

Chapter 2

Scattering theory at N/S interfaces

The first theoretical approach to describe the conductance of a N/S junction was developed by Blonder-Tinkham-Klapwijk (BTK)[32]. They used the Bogoliubov-de Gennes equations[19] and assumed ballistic transport. In order to take into account spin polarization[21, 22, 33], diffusive contacts[31, 37, 38], anisotropic superconducting order[39, 65, 41, 20], finite quasiparticle lifetime[42, 43, 44], external magnetic field[45], thin ferromagnetic layers at the interface[48] and the proximity effects[33] some extended BTK models have been proposed. An analysis of all these models is beyond the scope of this work, in this chapter we only introduce the BTK model and the attempt to include the proximity effects[33] in it.

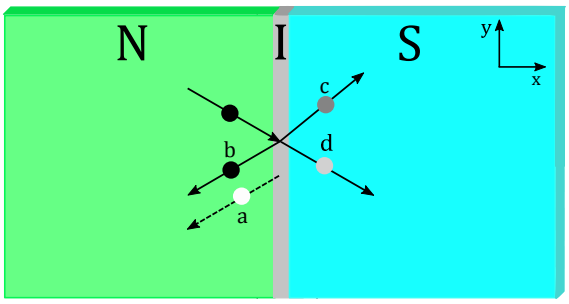

Figure 2.1: Scheme of the planar N/I/S junction and of the scattering processes that take place at the interface: Andreev reflection (a), normal reflection (b), transmission as electron-like quasiparticle (c) and transmission as hole-like quasiparticle (d).

2.1 Blonder Tinkham and Klapwijk model

We consider a planar NS junction, lying in the $xy-$plane, made up of a normal metal (N) connected to a superconductor (S) by a thin insulating barrier (I) (*see* Fig. 2.1). The scattering will be studied in the absence of magnetic fields ($\mathbf{A}(\mathbf{r}) = 0$) and we shall make a free particle approximation. We assume that the Fermi energy E_F and the effective mass m in the normal side of the junction ($x < 0$) are equal to those in the superconductor ($x > 0$), while the superconducting order parameter, assumed to be real, is taken of the form $\Delta(\mathbf{r}) = \Delta\theta(x)$, where $\theta(x)$ is the Heaviside step function and Δ is the BCS value of the energy gap. In absence of spin-flip scattering processes at the interface it is enough to solve 2×2 BdG equations

$$\begin{pmatrix} \mathcal{H}_0(\mathbf{r}) + V(\mathbf{r}) & \Delta(\mathbf{r}) \\ \Delta^*(x) & -(\mathcal{H}_0(\mathbf{r}) + V(\mathbf{r}))^* \end{pmatrix} \begin{pmatrix} u(\mathbf{r}) \\ v(\mathbf{r}) \end{pmatrix} = E \begin{pmatrix} u(\mathbf{r}) \\ v(\mathbf{r}) \end{pmatrix}, \quad (2.1)$$

where $\psi(\mathbf{r}) = (u(\mathbf{r}), v(\mathbf{r}))^t$ is the BdG state, E is the energy of a quasiparticle measured from E_F and $\mathcal{H}_0(\mathbf{r})$ is the single-particle Hamiltonian given by

$$\mathcal{H}_0(\mathbf{r}) = \left[-\frac{\hbar^2}{2m}\nabla^2 - E_F \right]. \quad (2.2)$$

We model the barrier potential at the interface ($x = 0$) by a Dirac delta potential

$$V(\mathbf{r}) = U_0\delta(x), \quad (2.3)$$

where U_0 is the strength of the barrier potential. Translational invariance along the $\hat{\boldsymbol{y}}-$direction implies the conservation of the momentum parallel to the interface, thus we can separate the variables and write the solutions using plane waves, i.e. $\psi(\mathbf{r}) = \psi(x)\, e^{i\boldsymbol{k}_\parallel \cdot \boldsymbol{r}}$, reducing the effective dimensionality of the problem. In order to solve the Bogoliubov-de Gennes equations (Eq. (2.1)), BTK took the plane waves as trial wave functions

$$\begin{cases} u(x) = u_k e^{ikx} \\ v(x) = v_k e^{ikx} \end{cases}. \quad (2.4)$$

Inserting these expression into the Bogoliubov-de Gennes equations we have in the superconducting side

$$\begin{pmatrix} \frac{\hbar^2k^2}{2m} - E_F & \Delta \\ \Delta & -\frac{\hbar^2k^2}{2m} + E_F \end{pmatrix} \begin{pmatrix} u_k(x) \\ v_k(x) \end{pmatrix} = E \begin{pmatrix} u_k(x) \\ v_k(x) \end{pmatrix}. \quad (2.5)$$

To obtain non-trivial solution of the system (Eq. (2.5)), E must satisfy

$$E^2 = \left(\frac{\hbar^2 k^2}{2m} - E_F\right)^2 + \Delta^2. \tag{2.6}$$

The Eq. (2.6), that gives quasiparticles energy spectrum, admits two solutions. Since we are concerned with excitations above the ground state we consider only the solution therefore $E \geq 0$. As consequence the BCS coherence factors are

$$u_k^2 = 1 - v_k^2 = \begin{cases} \frac{1}{2}\left[1 \pm \frac{\sqrt{E^2-\Delta^2}}{E}\right] & \text{for} \quad E > \Delta \\ \frac{1}{2} e^{\pm i \arccos \frac{E}{\Delta}} & \text{for} \quad E < \Delta. \end{cases} \tag{2.7}$$

In the BTK appoach they defined, for the sake of convenience, the BCS coherence factor as

$$u^2 = 1 - v^2 = \frac{1}{2}\left[1 + \frac{\sqrt{E^2 - \Delta^2}}{E}\right]. \tag{2.8}$$

This notation differs from the usual BCS coherence factors in which u_k and v_k are not defined for $E < \Delta$. Solving Eq. (2.6) respect to wave vector k we obtain four solutions $\pm k_+$ associated with the electon-like quasiparticles and $\pm k_-$ associated with the hole-like quasiparticles, where $\hbar k_\pm = \sqrt{2m\left(E_F \pm \sqrt{E^2 - \Delta^2}\right)}$. The wave functions in the superconductive side for electron-like and hole-like quasiparticles are, respectively

$$\psi_{el}(x) = \begin{pmatrix} u \\ v \end{pmatrix} e^{\pm i k_+ x}, \tag{2.9a}$$

$$\psi_{hl}(x) = \begin{pmatrix} v \\ u \end{pmatrix} e^{\pm i k_- x}. \tag{2.9b}$$

In the normal region, where the energy gap is zero, the Bogoliubov-de Gennes equations are

$$\begin{pmatrix} \frac{\hbar^2 k^2}{2m} - E_F & 0 \\ 0 & -\frac{\hbar^2 k^2}{2m} + E_F \end{pmatrix} \begin{pmatrix} u_k(x) \\ v_k(x) \end{pmatrix} = E \begin{pmatrix} u_k(x) \\ v_k(x) \end{pmatrix}, \tag{2.10}$$

from which we get for the wave vectors two solutions $\pm k$ associated with the electrons, where $\hbar k = \sqrt{2m(E_F + E)}$, and two solutions $\pm q$ associated with holes, where $\hbar q = \sqrt{2m(E_F - E)}$. The wave functions in the normal side for electrons and holes are, respectively

$$\psi_e(x) = \begin{pmatrix} 1 \\ 0 \end{pmatrix} e^{\pm i k x}, \tag{2.11a}$$

$$\psi_h(x) = \begin{pmatrix} 0 \\ 1 \end{pmatrix} e^{\pm i q x}. \tag{2.11b}$$

The wave vectors of the wave functions in Eqs. (2.9) and (2.11) are chosen under the constraint that an incident particle at the interface of the junction can only produce transmitted particles with positive group velocity ($v_g = (1/\hbar)\, dE/dk$) and reflected particles with negative group velocity. Thus, for an electron coming from the N side of the junction, the incident, reflected and transmitted wave functions may be written as

$$\psi_i(x) = \begin{pmatrix} 1 \\ 0 \end{pmatrix} e^{ikx} \tag{2.12}$$

$$\psi_r(x) = a \begin{pmatrix} 0 \\ 1 \end{pmatrix} e^{-ikx} + b \begin{pmatrix} 1 \\ 0 \end{pmatrix} e^{-ikx} \tag{2.13}$$

$$\psi_t(x) = c \begin{pmatrix} u \\ v \end{pmatrix} e^{ik_+ x} + d \begin{pmatrix} v \\ u \end{pmatrix} e^{ik_- x}. \tag{2.14}$$

Here the coefficients a, b, c and d correspond, respectively, to Andreev reflection, normal reflection, transmission as electron-like (ELQ) and hole-like quasiparticle (HLQ) (*see* Fig. 2.1). Therefore, the wave function in the normal side is given by:

$$\psi_N(x) = \psi_i(x) + \psi_r(x), \tag{2.15}$$

while in the superconducting side of the junction, we have

$$\psi_S(x) = \psi_t(x). \tag{2.16}$$

A powerful simplification for the determination of the coefficients in the above wave functions is constituted by the so-called Andreev approximation, valid for low temperatures and low bias voltages compared to the Fermi energy, under which one assumes that transport takes place only near the Fermi level. This approximation corresponds to assume $(E, \Delta) \ll E_F$ and thus retain the lowest order in E/E_F and Δ/E_F. This is equivalent to approximate $k \simeq q \simeq k_+ \simeq k_- \simeq k_F$.

2.2 Boundary conditions

The boundary conditions at the interface allow to calculate the coefficients in Eqs. (2.15) and (2.16). The first is the continuity of the wave function at the interface, namely

$$\psi_S(0) = \psi_N(0). \tag{2.17}$$

The second boundary condition depends on the delta function potential that simulates the barrier. To obtain it we consider the BdG equations

$$\frac{\hbar^2\partial_x^2}{2m}\begin{pmatrix} -1 & 0 \\ 0 & 1 \end{pmatrix}\psi(x) + U_0\begin{pmatrix} 1 & 0 \\ 0 & -1 \end{pmatrix}\delta(x)\,\psi(x) + \begin{pmatrix} -(E_F+E) & \Delta(x) \\ \Delta^*(x) & (E_F-E) \end{pmatrix}\psi(x) = 0, \tag{2.18}$$

with $\psi(x) = (u(x), v(x))^t$. We integrate from $-\varepsilon$ to ε and then take the limit for $\varepsilon \to 0$, obtaining

$$\lim_{\varepsilon\to 0}\int_{-\varepsilon}^{\varepsilon}\partial_x^2\psi(x)\,dx = -\frac{2m}{\hbar^2}\left\{\lim_{\varepsilon\to 0}\int_{-\varepsilon}^{\varepsilon}U_0\begin{pmatrix} -1 & 0 \\ 0 & -1 \end{pmatrix}\delta(x)\,\psi(x)\,dx + \lim_{\varepsilon\to 0}\int_{-\varepsilon}^{\varepsilon}\begin{pmatrix} -(E_F+E) & \Delta(x) \\ \Delta^*(x) & (E_F-E) \end{pmatrix}\psi(x)\,dx\right\}, \tag{2.19}$$

which reduces, for the continuity of the wave function $\psi(x)$, to:

$$\partial_x\psi\left(0^+\right) - \partial_x\psi\left(0^-\right) = 2k_F Z_0\begin{pmatrix} 1 & 0 \\ 0 & 1 \end{pmatrix}\psi(0), \tag{2.20}$$

namely

$$\partial_x\psi_S\Big|_{x=0} - \partial_x\psi_N\Big|_{x=0} = 2k_F Z_0\begin{pmatrix} 1 & 0 \\ 0 & 1 \end{pmatrix}\psi_S(0), \tag{2.21}$$

where $Z_0 = mU_0/\hbar^2 k_F$ is a dimensionless parameter that describes the transparency of the interface. To understand the meaning of the parameter Z_0 it is enough to note that the transmission coefficient in the normal state (i.e. for a N/N junction) is given by $(1+Z_0^2)^{-1}$ and the corresponding reflection coefficient is $Z_0^2/(1+Z_0^2)$. Using the above conditions on the wave functions we obtain the following four equations

$$\begin{aligned} &b - cu - dv = -1 \\ &a - cv - du = 0 \\ &ikb + (ik_+u - 2k_F Z_0 u)\,c + (-ik_-v - 2k_F Z_0 v)\,d = 0 \\ -&iqa + (ik_+v - 2k_F Z_0 v)\,c + (-ik_-u - 2k_F Z_0 u)\,d = 0. \end{aligned} \tag{2.22}$$

Making use of the Andreev approximation ($k \simeq q \simeq k_+ \simeq k_- \simeq k_F$), we find the following expression for the scattering coefficients

$$\begin{aligned} a &= \frac{uv}{\gamma} \\ b &= -\frac{(u^2 - v^2)\left[Z_0\left(2i + Z_0\right)\right]}{\gamma} \\ c &= \frac{2u\left(2 - iZ_0\right)}{\gamma} \\ d &= \frac{2ivZ_0}{\gamma}, \end{aligned} \tag{2.23}$$

where $\gamma = u^2 + Z_0^2\left(u^2 - v^2\right)$.
Let us note that in the absence of a barrier (i.e. $Z_0 = 0$) $b = d = 0$. Physically this means that all reflection is Andreev reflection and all transmission is electron-like quasiparticle transmission.

2.3 Probability current density

In Nambu space (electron-hole space), as in ordinary quantum mechanics[36], a probability current density can be associated to the wave function. It is given by

$$\mathbf{J}\left(\mathbf{r}\right) = \frac{\hbar}{m}\,\mathrm{Im}\left\{\psi^{\dagger}\left(\mathbf{r}\right)\nabla\psi\left(\mathbf{r}\right)\right\} = \frac{\hbar}{m}\,\mathrm{Im}\left\{u^{*}\left(\mathbf{r}\right)\nabla u\left(\mathbf{r}\right) - v^{*}\left(\mathbf{r}\right)\nabla v\left(\mathbf{r}\right)\right\}, \tag{2.24}$$

that satisifies the continuity equation

$$\frac{\partial P\left(\mathbf{r},t\right)}{\partial t} + \nabla\cdot\mathbf{J}\left(\mathbf{r}\right) = 0, \tag{2.25}$$

where $P\left(\mathbf{r},t\right) = \left|\psi\left(\mathbf{r}\right)\right|^2 = \left|u\left(\mathbf{r}\right)\right|^2 + \left|v\left(\mathbf{r}\right)\right|^2$ is the probability of finding either, at time t in a volume element $d\mathbf{r}$ situated at the point $\mathbf{r}$, an electron-like quasiparticle or a hole-like quasiparticle. It is interesting to note that in Eq. (2.24) hole current enters with a sign opposite to that of the electron part. Through $\mathbf{J}\left(\mathbf{r}\right)$ we can derive the probability amplitudes associated to the coefficients contained in the wave functions (Eqs. (2.15) and (2.16)). We indicate with $A\left(E\right)$ the probability associated with the Andreev reflection, $B\left(E\right)$ the probabilty associated with normal reflection, $C\left(E\right)$ the probability associated with the transmission as ELQ and $D\left(E\right)$ the probability associated with the transmission as HLQ. These must fulfill the normalization condition of the total probability

$$A\left(E\right) + B\left(E\right) + C\left(E\right) + D\left(E\right) = 1. \tag{2.26}$$

The explicit expressions for $A(E)$, $B(E)$, $C(E)$ and $D(E)$ are derived from the conservation of the probability current density

$$\mathbf{J}_{TOT} = 0, \tag{2.27}$$

namely

$$\mathbf{J}_I + \mathbf{J}_A + \mathbf{J}_R = \mathbf{J}_T^C + \mathbf{J}_T^D, \tag{2.28}$$

from which follows

$$1 = -\frac{\mathbf{J}_A}{\mathbf{J}_I} - \frac{\mathbf{J}_R}{\mathbf{J}_I} + \frac{\mathbf{J}_T^C}{\mathbf{J}_I} + \frac{\mathbf{J}_T^D}{\mathbf{J}_I}. \tag{2.29}$$

Here with $\mathbf{J}_I$, $\mathbf{J}_A$, $\mathbf{J}_R$, $\mathbf{J}_T^C$ and $\mathbf{J}_T^D$ we indicate, respectively, the probability density current associated with the incident particle, Andreev reflection, the normal reflection, the transmission as ELQ and the transmission as HLQ. These density current probabilities can be obtained inserting the wave functions $\psi_i(x)$ (Eq. 2.12), $\psi_r(x)$(Eq. 2.13) and $\psi_t(x)$(Eq. 2.14) in Eq. (2.24)

- $\mathbf{J}_I = \frac{\hbar}{m} \operatorname{Im}\left\{\psi_i^\dagger \nabla \psi_i\right\}$, with $\psi_i(x) = \begin{pmatrix} 1 \\ 0 \end{pmatrix} e^{ikx}$

$$\mathbf{J}_I = \frac{\hbar k}{m}, \tag{2.30}$$

- $\mathbf{J}_A = \frac{\hbar}{m} \operatorname{Im}\left\{\psi_r^\dagger \nabla \psi_r\right\}$, with $\psi_r(x) = a \begin{pmatrix} 0 \\ 1 \end{pmatrix} e^{iqx}$

$$\mathbf{J}_A = -\frac{\hbar q}{m}|a|^2, \tag{2.31}$$

$$A(E) = \left|\frac{\mathbf{J}_A}{\mathbf{J}_I}\right| = \frac{q}{k}|a|^2, \tag{2.32}$$

- $\mathbf{J}_R = \frac{\hbar}{m} \operatorname{Im}\left\{\psi_r^\dagger \nabla \psi_r\right\}$, with $\psi_r(x) = b \begin{pmatrix} 1 \\ 0 \end{pmatrix} e^{-ikx}$

$$\mathbf{J}_R = -\frac{\hbar k}{m}|b|^2, \tag{2.33}$$

$$B(E) = \left|\frac{\mathbf{J}_R}{\mathbf{J}_I}\right| = |b|^2, \tag{2.34}$$

- $\mathbf{J}_T^C = \dfrac{\hbar}{m}\,\mathrm{Im}\left\{\psi_t^\dagger \nabla \psi_t\right\}, \quad \text{with} \quad \psi_t(x) = c\begin{pmatrix} u \\ v \end{pmatrix} e^{ik_+ x}$

$$\mathbf{J}_T^C = \frac{\hbar k_+}{m}\left(u^2 - v^2\right)|c|^2, \tag{2.35}$$

$$C(E) = \left|\frac{\mathbf{J}_T^C}{\mathbf{J}_I}\right| = \frac{k_+}{k}\left(|u|^2 - |v|^2\right)|c|^2, \tag{2.36}$$

- $\mathbf{J}_T^D = \dfrac{\hbar}{m}\,\mathrm{Im}\left\{\psi_t^\dagger \nabla \psi_t\right\}, \quad \text{with} \quad \psi_t(x) = d\begin{pmatrix} v \\ u \end{pmatrix} e^{-ik_- x}$

$$\mathbf{J}_T^D = \frac{\hbar k_-}{m}\left(u^2 - v^2\right)|d|^2, \tag{2.37}$$

$$D(E) = \left|\frac{\mathbf{J}_T^D}{\mathbf{J}_I}\right| = \frac{k_-}{k}\left(|u|^2 - |v|^2\right)|d|^2. \tag{2.38}$$

In the Andreev approximation the probability amplitudes become $A(E) = |a|^2$, $B(E) = |b|^2$, $C(E) = \left(|u|^2 - |v|^2\right)|c|^2$ and $D(E) = \left(|u|^2 - |v|^2\right)|d|^2$. Therefore, the probability current density on the N side in units of k_F is

$$\mathbf{J}_N = \mathbf{J}_I + \mathbf{J}_A + \mathbf{J}_R = \frac{\hbar k_F}{m}\left(1 - |a|^2 - |b|^2\right), \tag{2.39}$$

while the probability current density on the S side is

$$\mathbf{J}_S = \mathbf{J}_T^C + \mathbf{J}_T^D = \frac{\hbar k_F}{m}\left(|u|^2 - |v|^2\right)\left(|c|^2 + |d|^2\right). \tag{2.40}$$

For $E > \Delta$, u and v are real so the probability amplitudes assume the following form:

$$\begin{cases} A = \dfrac{u^2 v^2}{\gamma^2} \\ B = \dfrac{\left(u^2 - v^2\right)^2 Z_0^2\left(1 + Z_0^2\right)}{\gamma^2} \\ C = \dfrac{u^2\left(u^2 - v^2\right)\left(1 + Z_0^2\right)}{\gamma^2} \\ D = \dfrac{v^2}{\gamma^2}\left(u^2 - v^2\right) Z_0^2 \end{cases}, \tag{2.41}$$

while for $E < \Delta$, u and v are complex conjugates and we have

$$\begin{cases} A = \dfrac{\Delta^2}{E^2 + (\Delta^2 - E^2)\left(1 + 2Z_0^2\right)^2} \\ B = \dfrac{(E^2 - \Delta^2)\left[1 + (1 + 2Z_0^2)^2\right]}{E^2 + (\Delta^2 - E^2)\left(1 + 2Z_0^2\right)^2} \\ C = 0 \\ D = 0 \end{cases} . \tag{2.42}$$

In the case (Eq. (2.42)), $C = D = 0$, there is the absence of transmission because the energy of the incident electron does not sufficient to excite particles in the superconducting side. In general A, B, C and D depend on the angle of incidence of the incoming electron and on the detailed shape of the scattering potential. In Fig. 2.2 we show A, B, C and D *vs* E/Δ for different values of Z_0. Except for $Z_0 = 0$, $A(E)$ has a sharp peak for $E = \Delta$,

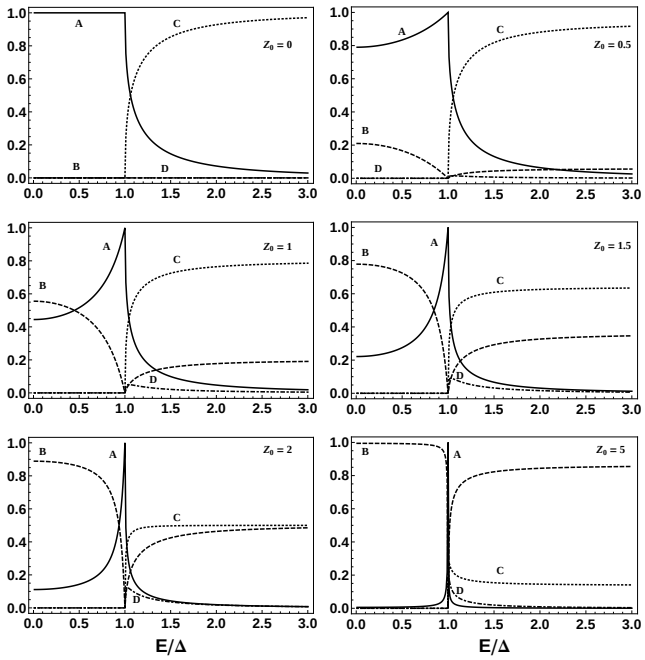

Figure 2.2: Plots of the probability amplitudes associated with Andreev reflection A (full line), normal reflection B (dashed line), transmissions as ELQ C (dotted line) and as HLQ D (dot-dashed line). The curves are obtained for distinct values of Z_0 ranging from metallic to the tunnel regime.

although this peak becomes very narrow with increasing of Z_0. For $Z_0 = 0$ and $E < \Delta$ only possible process is Andreev reflection, while for $E > \Delta$ is

also possible the transmission as ELQ. With increasing of Z_0, for $E < \Delta$ Andreev reflection and the normal reflection are possible, while for $E > \Delta$ are also possible the transmission as ELQ and HLQ.

2.4 Current and differential conductance

When a voltage is applied, nonequilibrium quasiparticle populations will be generated, which can be described by self-consistent solution to the Boltzmann equation. This solution is greatly simplified in the ballistic transport regime, where are considered scatterings only at N/S interface. This assumption enables to adopt that, even under nonequilibrium conditions, the distribution functions of the particles are given by equilibrium Fermi-Dirac distribution. Choosing as reference energy the electrochemical potential of the Cooper pairs in the superconductor, we have that all incoming electrons from the S side have the distribution function $f(E)$, while those coming in from the N side are described by $f(E - eV)$. It is more convenient to calculate the current on the N side, where all current is carried by either electrons or holes and not Cooper pairs. The current is given by

$$I_{NS} = 2ev_F N(E_F) \mathscr{A} \int_{-\infty}^{+\infty} [f_{\rightarrow}(E) - f_{\leftarrow}(E)]\, dE, \tag{2.43}$$

where 2 is the spin degeneracy factor, e is the electron charge, v_F is the Fermi velocity, $N(E_F)$ is the density of states at the Fermi energy, $\mathscr{A}$ is the effective-neck cross-sectional area. With the assumptions made above, we can write

$$\begin{aligned} f_{\rightarrow}(E) &= f(E - eV) && (2.44) \\ f_{\leftarrow}(E) &= A(E)[1 - f_{\rightarrow}(-E)] + B(E) f_{\rightarrow}(E) \\ &+ [C(E) + D(E)] f(E). && (2.45) \end{aligned}$$

Let us note that the Andreev term is is multiplied by $1 - f_{\rightarrow}(-E)$ which represents the probability that an incident hole with energy $-E$ will Andreev reflected and emerge as an electron with energy E. By employing the properties that $A(E) + B(E) + C(E) + D(E) = 1$, $f(-E) = 1 - f(E)$ and $A(E) = A(-E)$ we obtain

$$I_{NS} = 2ev_F N(E_F) \mathscr{A} \int_{-\infty}^{+\infty} [f(E - eV) - f(E)][1 + A(E) - B(E)] dE. \tag{2.46}$$

The quantity $[1 + A(E) - B(E)]$ is called the transmission coefficient for electrical current. Its expression shows that while normal reflection (described by $B(E)$) reduces the current, Andreev reflection (described by

$A(E)$) increases it by giving rise to two transferred electrons (a Cooper pair) for incident one. If both side of the junction are normal metal, $A = 0$ since there is no Andreev reflection, $C = 1 - B = (1 + Z_0^2)^{-1}$, so that Eq. (2.46) reduces to the simple form

$$I_{NN} = \frac{2e^2 v_F N(E_F) \mathscr{A}}{1 + Z_0^2} V = \frac{V}{R_N}, \tag{2.47}$$

where R_N is the normal state resistance, that is nonzero even in the absence of a barrier ($Z_0 = 0$). The differential conductance is defined as the derivative of the current with respect to voltage (dI_{NS}/dV)

$$G(V) = 2ev_F N(E_F) \mathscr{A} \int dE \left[1 + A(E) - B(E)\right] \left[-\frac{\partial f(E - eV)}{\partial E}\right]. \tag{2.48}$$

At $T = 0$ the derivative of the Fermi-Dirac distribution function reduces to a Dirac delta function and the differential conductance becomes

$$G(V) = 2ev_F N(E_F) \mathscr{A} \left[1 + A(eV) - B(eV)\right] \tag{2.49}$$

The behavior of the differential conductance G/G_N *vs* E/Δ, with $G_N = G(eV \gg \Delta)$, is shown at $T = 0$ (Fig. 2.3) and at finite temperature (Fig. 2.4) for different values of interfacial barrier strength Z_0. For $Z_0 = 0$ and for $E < \Delta$, $G/G_N = 2$, as consequence an incidente particle at the interface gets completely reflected as hole, then is possible only Andreev reflection. On other hand, for $E > \Delta$ the transmission as ELQ is possible and $G/G_N < 2$. For $Z_0 > 1$ the normal reflection dominates everywhere except near the gap, where occurs the peak due to Andreev reflection. Then, the effect of the barrier Z_0 is to suppress the conductance everywhere except for $E = \Delta$, while that of the finite temperature is to smear the sharp features evident at $T = 0$.

2.5 Proximity model

In this section we summarize the principal results of the model proposed by Strijkers *et al.*[33]. It is well-known that at the interface between superconducting and non-superconducting materials a superconducting region is created due to the diffusion of the Cooper pairs from the superconducting material. This superconducting proximity region has a lower transition temperature and a lower energy gap than those of the bulk. These effects are incorporated in the BTK model by introducing two gap values, Δ_1 related to the Andreev reflection process, and Δ_2 that describes the quasiparticle

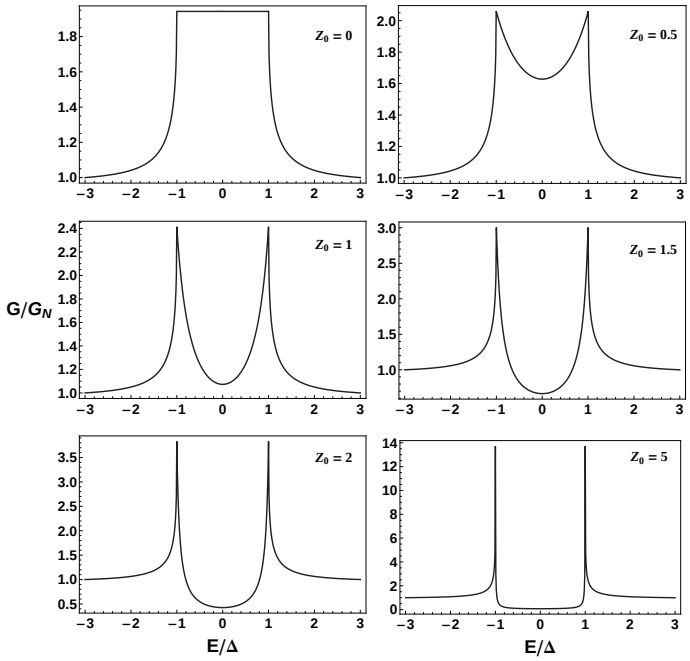

Figure 2.3: Normalized differential conductance curves, G/G_N *vs* E/Δ, calculated a $T = 0$. The different curves are obtained for values of Z_0 ranging from metallic limit to the tunnel regime.

transport[33]. Quasiparticles can enter the superconductor only for energies larger than Δ_2 and Andreev reflection is limited to energies smaller than Δ_1. Therefore the scattering problem can be divided into three different energy ranges: energy inside of the gap, energy outside of the gap and energy between Δ_1 and Δ_2. With these assumptions they find the resulting expression for the probabilities associated to the Andreev and normal reflection for:

- $|E| \leq \Delta_1$

$$\begin{cases} A = \frac{\Delta_1^2}{E^2+\left(\Delta_1^2-E^2\right)\left(1+2Z^2\right)^2} \\ B = 1 - A \end{cases} \tag{2.50}$$

- $\Delta_1 < |E| < \Delta_2$

$$\begin{cases} A = \frac{u_1^2 v_1^2}{\gamma_1^2} \\ B = 1 - A \end{cases} \tag{2.51}$$

- $\Delta_2 \leq |E|$

$$\begin{cases} A = \frac{u_1^2 v_1^2}{\gamma_1^2} \\ B = \frac{\left(u_2^2-v_2^2\right)^2 Z^2\left(1+Z^2\right)}{\gamma_2^2} \end{cases} \tag{2.52}$$

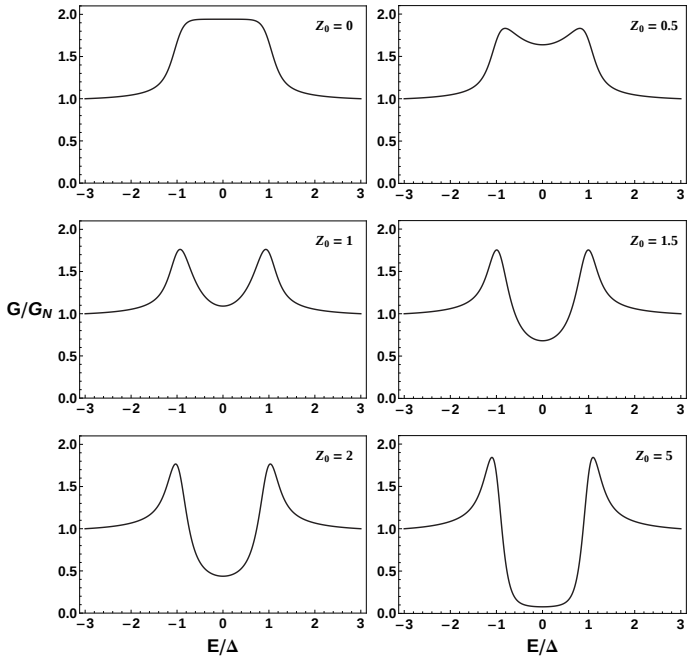

Figure 2.4: Normalized differential conductance curves, G/G_N *vs* E/Δ, calculated a $T = 1.6K$. The different curves are obtained for values of Z_0 ranging from metallic limit to the tunnel regime.

where

$$u_1^2 = 1 - v_1^2 = (1/2)\left\{\left[\left(E^2 - \Delta_1^2\right)/E^2\right]^{1/2}\right\} \quad (2.53)$$

$$u_2^2 = 1 - v_2^2 = (1/2)\left\{\left[\left(E^2 - \Delta_2^2\right)/E^2\right]^{1/2}\right\} \quad (2.54)$$

$$\gamma_1^2 = \left(u_1^2 + Z^2\left[u_1^2 - v_1^2\right]\right)^2 \quad (2.55)$$

$$\gamma_2^2 = u_1^2 v_1^2 + \left(u_2^2 - v_2^2\right)\left[u_2^2 + Z^2 + \left(u_2^2 - v_2^2\right)Z^2\left(1 + Z^2\right)\right] \quad (2.56)$$

and Z describes the strength of the barrier potential at the interface.
The differential conductance is given by the standard formula (Eq. 2.48) and is calculated by substituting the expressions of probability amplitudes associated to Andreev and normal reflection shown in Eqs. ((2.50) - (2.52)). Fig. 2.5 shows two curves of the normalized differential conductance G/G_N as function of bias voltage V. For $Z = 0$, $\Delta_1 = \Delta_2$ the usual BTK behavior is recovered (left panel of Fig. 2.5), while for $\Delta_1 \neq \Delta_2$ a zero-bias peak with two sharp dips at the position of the superconducting bulk gap appears (right panel of Fig. 2.5), due to the proximity-induced superconducting region of the normal metal. We name the model with the two gaps Δ_1 and Δ_2 the proximity model. In next chapter we will propose a different generalization

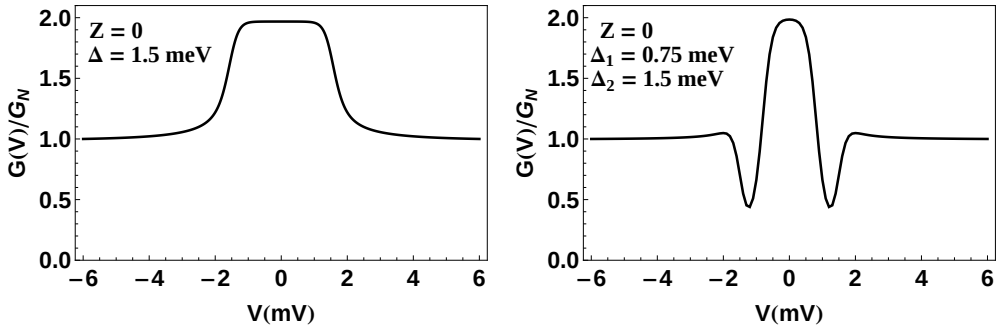

Figure 2.5: Normalized differential conductance curves, G/G_N *vs* V, calculated at $T = 1.5K$ with Z, Δ_1 and Δ_2 as shown in the figure. In the left panel $\Delta_1 = \Delta_2 = \Delta$.

of the BTK theory to include the proximity effects introducing a particle-hole mixing term in the interface potential.

Chapter 3

Generalization of the BTK model

In this chapter we extend the BTK theory to include non-diagonal boundary conditions[47] (in particle-hole space) in the BdG scattering problem, by introducing an interface potential that mixes electron and hole components. We show that this potential describes the proximity effect at the interface and it is responsible for the formation of conductance dips in the differential conductance spectra of N/S junctions. In the original form of the BTK theory the description of interface effects takes place through a localized scattering potential, whose strength is quantified by the parameter Z. From a mathematical point of view, including a Dirac delta potential within the BdG formalism, used in the BTK model, produces matching conditions of the scattering problem diagonal in the particle-hole representation. However, off-diagonal boundary conditions in the Nambu space are also mathematically allowed in the BdG formalism. Apart from the mathematical motivation, the need to take into account general boundary conditions for a BdG scattering problem arises from the occurence of anomalous features in the measured PCAR conductance spectra. Indeed, these experiments [21, 33, 20, 48, 49, 50, 51, 35] report conductance dips and anomalous values of the zero-bias conductance (ZBC), not expected in the standard BTK formalism. Thus, a certain number of the mentioned anomalies could be recovered simply generalizing the boundary conditions of the scattering problem.

3.1 Model

We consider one-dimensional N/S junction described by the BdG equations

$$\left[\mathcal{H} + V\left(x\right)\right]\psi\left(x\right) = E\psi\left(x\right), \tag{3.1}$$

where $\psi(x) = (u_\uparrow(x), u_\downarrow(x), v_\uparrow(x), v_\downarrow(x))^t$ is the quasiparticle state associate to the excitation energy E above the Fermi energy E_F. The Hamiltonian $\mathcal{H}$, which describes the bulk properties of the junction is

$$\mathcal{H} = \begin{pmatrix} \hat{H}_0 & i\hat{\sigma}_y\Delta(x) \\ -i\hat{\sigma}_y\Delta^*(x) & -\hat{H}_0^* \end{pmatrix}, \tag{3.2}$$

where the single-particle Hamiltonian operator $\hat{H}_0$ is defined by

$$\hat{H}_0 = \left[-\frac{\hbar^2}{2m}\partial_x^2 - E_F\right]\hat{\mathbb{I}}, \tag{3.3}$$

with $\hat{\mathbb{I}}$ the identity operator in the spin space and $\hat{\sigma}_y$ the Pauli matrix. We assume that the Fermi energy E_F and the effective mass m in the normal side of the junction ($x < 0$) are equal to those in the superconductor ($x > 0$). The barrier potential at the interface ($x = 0$) is modelled as

$$V(x) = \begin{pmatrix} U_0\hat{\mathbb{I}} & iU_1\hat{\sigma}_y e^{i\varphi} \\ -iU_1\hat{\sigma}_y e^{-i\varphi} & -U_0\hat{\mathbb{I}} \end{pmatrix}\delta(x), \tag{3.4}$$

where U_0 indicates the usual BTK barrier strength, while the term U_1 describes the interfacial electron-hole coupling strength. The off-diagonal components of $V(x)$ describe the presence of a weak superconducting interface[27] which can be intuitively understood in terms of proximity effect. The variable φ represents the phase difference between the interface and the bulk superconducting order parameter. Maintaining arbitrary values of φ, a Josephson current $I_J(\varphi) \propto \sin(\varphi)$[52] is expected to flow through the interface. The free energy of the system is expected to be minimized when Josephson current vanishes, i.e. for $\varphi = 0$ or π, the value $\varphi = 0$ being a free energy minimum of the N/S junction. On the other hand, the value $\varphi = \pi$ can become an energy minimum if a magnetic moment is formed at the interface. For instance, the transition metals easily oxidize producing localized magnetic states. This can be in principle the case of Cu/Nb junctions, where the presence of localized magnetic states[53] at the interface cannot be excluded. If the magnetic moment at the interface is sufficiently strong, the interfacial phase φ can be modified from the value $\varphi = 0$ to $\varphi = \pi$ and the sign change of the interfacial order parameter follows a mechanism similar to the one described by Kontos *et al.*[54].

3.2 Solutions of Bogoliubov-de Gennes equations

The wave function of an electron with spin $\sigma =\uparrow,\downarrow$ coming from the N-side of the junction is given by:

$$\begin{aligned}\psi_N^\sigma(x) &= \begin{pmatrix}\delta_{\uparrow\sigma}\\ \delta_{\downarrow\sigma}\\ 0\\ 0\end{pmatrix} e^{ikx} + r_e^\uparrow \begin{pmatrix}1\\ 0\\ 0\\ 0\end{pmatrix} e^{-ikx} + r_e^\downarrow \begin{pmatrix}0\\ 1\\ 0\\ 0\end{pmatrix} e^{-ikx} \\ &+ r_h^\uparrow \begin{pmatrix}0\\ 0\\ 1\\ 0\end{pmatrix} e^{iqx} + r_h^\downarrow \begin{pmatrix}0\\ 0\\ 0\\ 1\end{pmatrix} e^{iqx}. \end{aligned} \tag{3.5}$$

Here the coefficients $r_e^{\uparrow,\downarrow}$ and $r_h^{\uparrow,\downarrow}$ correspond, respectively, to normal reflection and Andreev reflection, while $\hbar k = \sqrt{2m\left(E_F + E\right)}$ and $\hbar q = \sqrt{2m\left(E_F - E\right)}$ indicate the electron and hole wave vectors.
In the superconducting region, we have

$$\begin{aligned}\psi_S(x) &= t_e^\uparrow \begin{pmatrix}u\\ 0\\ 0\\ v\end{pmatrix} e^{ik_+x} + t_e^\downarrow \begin{pmatrix}0\\ u\\ -v\\ 0\end{pmatrix} e^{ik_+x} + t_h^\downarrow \begin{pmatrix}v\\ 0\\ 0\\ u\end{pmatrix} e^{-ik_-x} \\ &+ t_h^\uparrow \begin{pmatrix}0\\ v\\ -u\\ 0\end{pmatrix} e^{-ik_-x}, \end{aligned} \tag{3.6}$$

where the coefficients $t_e^\uparrow$, $t_e^\downarrow$, $t_h^\uparrow$, $t_h^\downarrow$ correspond to the transmission as electron-like and hole-like quasiparticle with wave vectors $\hbar k_\pm = \sqrt{2m\left(E_F \pm \sqrt{E^2 - \Delta^2}\right)}$, the BCS[14] coherence factors being

$$u^2 = 1 - v^2 = \frac{1}{2}\left(1 + \frac{\sqrt{E^2 - \Delta^2}}{E}\right). \tag{3.7}$$

3.3 Boundary conditions

The boundary conditions at the interface allow for the calculation of the coefficients in Eqs. (3.5) and (3.6). The first is that the wave functions have

to be continuous at the interface. The second, that depends on the potential at the interface, it can be extracted by integrating the BdG equations from $x = -\epsilon$ to $x = \epsilon$ and then letting $\epsilon \to 0$. Thus we get:

$$\partial_x \psi\left(0^+\right) - \partial_x \psi\left(0^-\right) = \frac{2m}{\hbar^2}\left[\begin{pmatrix} U_0\hat{\mathbb{I}}_{2\times 2} & iU_1\hat{\sigma}_y e^{i\varphi} \\ iU_1\hat{\sigma}_y e^{-i\varphi} & U_0\hat{\mathbb{I}}_{2\times 2} \end{pmatrix}\right]\psi\left(0\right). \tag{3.8}$$

Finally the boundary conditions are:

$$\begin{aligned} \psi_N^\sigma\left(0\right) &= \psi_S\left(0\right) \\ \partial_x\psi_S|_{x=0} - \psi_N^\sigma|_{x=0} &= \mathcal{A}\psi\left(0\right). \end{aligned} \tag{3.9}$$

The matching matrix

$$\mathcal{A} = k_F Z_0 \hat{\mathbb{I}}_{4\times 4} + k_F Z_1 \begin{pmatrix} 0 & i\hat{\sigma}_y e^{i\varphi} \\ i\hat{\sigma}_y e^{-i\varphi} & 0 \end{pmatrix} \tag{3.10}$$

contains a diagonal term in the electron-hole representation with the usual BTK parameter $Z_0 = 2mU_0/\hbar^2 k_F$ and off-diagonal terms of strength $Z_1 = 2mU_1/\hbar^2 k_F$. The physical meaning and the range of variability of the particle-hole mixing parameter Z_1 will be discussed in Sec. 3.7. Using the above boundary conditions on the wave functions (Eqs. (3.5) and (3.6)) and the Andreev approximation, we find the following coefficients assuming the injection of a spin-up (the result does not depend on the spin of the incoming process) electron from the normal side

$$\begin{aligned} r_h^\downarrow &= \frac{4uv - 2ie^{-i\varphi}Z_1(u^2-v^2)}{4u^2 + 4iuvZ_1\cos\varphi + (u^2-v^2)(Z_0^2+Z_1^2)} \\ r_e^\uparrow &= -\frac{4iuvZ_1\cos\varphi + (u^2-v^2)[Z_0(2i+Z_0)+Z_1^2)]}{4u^2 + 4iuvZ_1\cos\varphi + (u^2-v^2)(Z_0^2+Z_1^2)} \\ t_e^\uparrow &= \frac{4u - 2i(uZ_0 - vZ_1e^{-i\varphi})}{4u^2 + 4iuvZ_1\cos\varphi + (u^2-v^2)(Z_0^2+Z_1^2)} \\ t_h^\downarrow &= \frac{2i(vZ_0 - uZ_1e^{-i\varphi})}{4u^2 + 4iuvZ_1\cos\varphi + (u^2-v^2)(Z_0^2+Z_1^2)}, \end{aligned} \tag{3.11}$$

while the absence of spin-flip scattering implies $r_e^\downarrow = r_h^\uparrow = t_e^\downarrow = t_h^\uparrow = 0$.

3.4 Differential conductance

Once all the transmission and reflection probabilities are obtained, we can calculate the differential conductance by the formula

$$G(V) \propto \sum_\sigma \int dE \left[1 + |r_h^{\bar{\sigma}}\left(E\right)|^2 - |r_e^\sigma\left(E\right)|^2\right]\left[-\frac{\partial f(E-eV)}{\partial E}\right] \tag{3.12}$$

where the quantities $\{r_h^\sigma, r_e^\sigma\}$ are the Andreev reflection and normal reflection probabilities, respectively, $f(E)$ is the Fermi-Dirac distribution, while the notation $\bar{\sigma}$ indicates the spin polarization opposite to σ. To illustrate the effects of the barrier strengths Z_0, Z_1 and of the phase φ we plot the finite temperature conductance of the N/S junction. In Figure 3.1 we show the normalized conductance G/G_N *vs* E/Δ, with $G_N = G(eV \gg \Delta)$, for different values of Z_0 and Z_1 at a fixed temperature $T = 1.6K$, computed by using Eq. (3.12). Two cases are considered: (i) $\varphi = 0$, shown in the left panels; (ii) $\varphi = \pi$, shown in the right panels. In each plot, different curves correspond to different Z_0 values (ranging from 0 to 2), while Z_1 is fixed as labelled. For $\varphi = 0$ and $Z_1 = 0$ (Figure 3.1(a)) the usual BTK behavior is recovered. In this case, the zero-bias conductance is suppressed as Z_0 is increased, while two peaks at $E/\Delta \approx \pm 1$ appear. Fixing $Z_1 = 0.5$ (Fig. 3.1(c)), we observe a reduction of the amplitude of the zero-bias conductance (ZBC) feature compared to the $Z_1 = 0$ case. The difference between the conductance lowering induced by Z_0 and the peculiar amplitude reduction induced by Z_1 is evident: while the increasing of Z_0 induces a zero-bias conductance minimum, a tendency to increase the zero-bias conductance is observed by rising Z_1 to 1.0 (Fig. 3.1(e)), $Z_1 = 1.5$ (Fig.3.1(g)) and $Z_1 = 2$ (Fig. 3.1(i)). A different scenario is observed for $\varphi = \pi$: the effect of moderate values of Z_1, namely $Z_1 = 0.5$ (Fig. 3.1(d)) and $Z_1 = 1$ (Fig. 3.1(f)), combine with Z_0 to give a relevant effective barrier strength leading to a strong suppression of the sub-gap conductance up to fully gapped spectra. For $Z_1 = 1.5$ (Fig. 3.1(h)) and $Z_1 = 2$ (Fig. 3.1(l)) an evident zero-bias peak surrounded by two dips at $E/\Delta \approx \pm 1$ appears. Such ZBC peak exists for all Z_0 values in the range $[0, 2]$, the junction transparency reduction having effect only on the peak amplitude. All the conductance structures presented above (coming from the generalized boundary conditions) cannot be recovered within the standard BTK approach (except for the case $Z_1 = 0$).

3.5 Comparison with the proximity model

To show the relevance of this approach, we compare the temperature evolution of the conductance spectra (Fig. 3.2) obtained in the generalized BTK model introduced above, with the one calculated by using the transmission and reflection coefficients of the proximity model of Strijker *et al.* [33] characterized by the barrier height Z and two gap values at the interface Δ_1, describing the proximity effect at the interface, and Δ_2 related to the superconducting bulk. Both models can be used to reproduce (black solid lines in Fig. 3.2(a) and 3.2(b)) the experimental data reported for

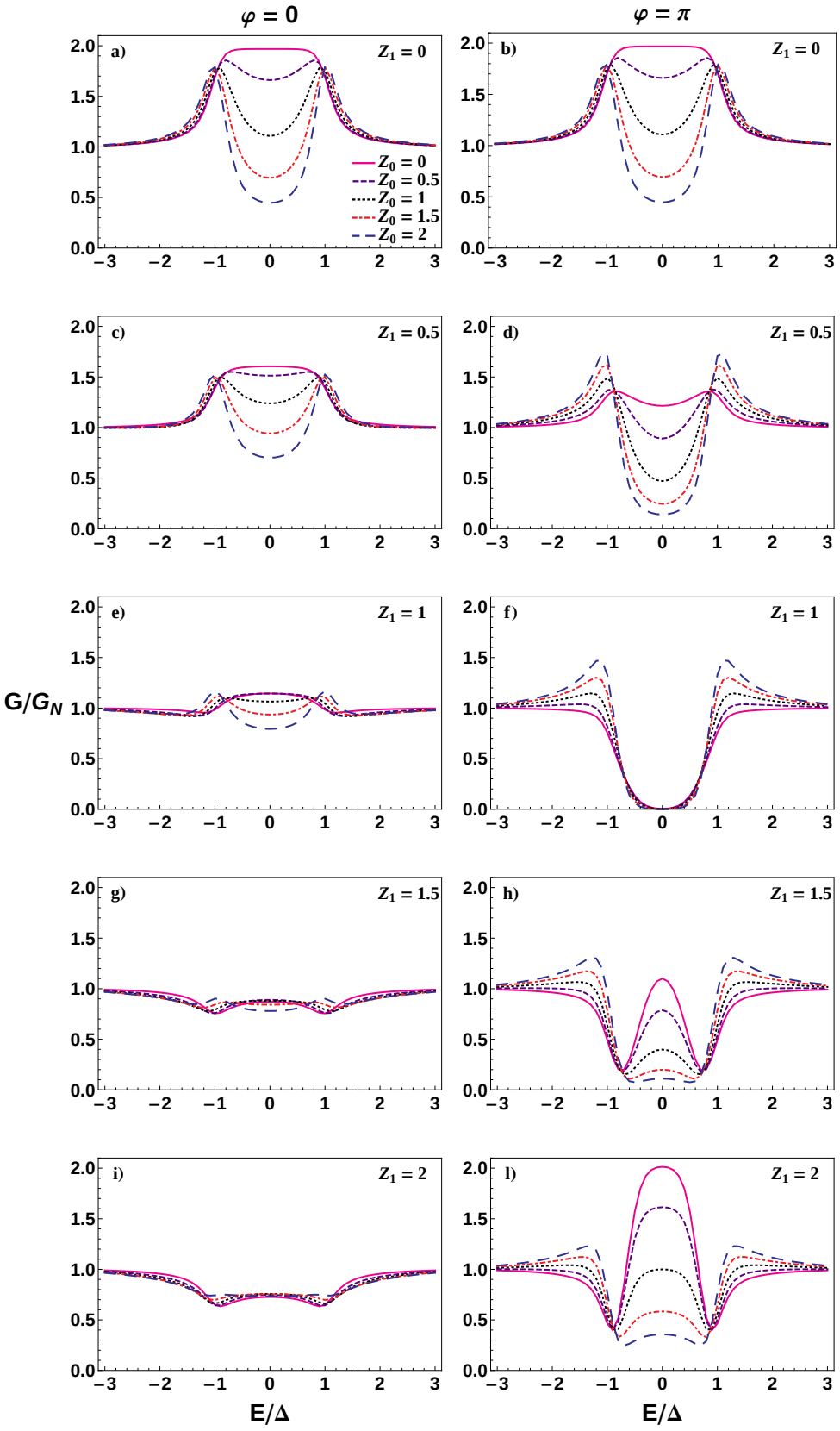

Figure 3.1: Normalized differential conductance curves, G/G_N *vs* E/Δ, calculated at $T = 1.6K$. The different curves are obtained for distinct values of Z_0, Z_1 and φ (values in the panels).

Cu/Nb contacts in Ref.[33]. In particular, in Fig. 3.2(a) we show theoretical curves calculated in the temperature range between $0.1K$ and $5.2K$ by assuming $Z_0 = 0.25$, $Z_1 = 2$, $\Delta = 1.5meV$, $\varphi = \pi$, while in Fig. 3.2(b) the conductance curves are obtained by considering the parameters $Z = 0.14$, $\Delta_1 = 0.99meV$, $\Delta_2 = 0.47meV$, in the proximity model. For both the theoretical curves is necessary to fix a temperature value of $0.9K$, that is lower than the bath temperature and it has been motivated as the result of non-equilibrium effects [33] as well as in terms of other physical effects [55]. Let us note that the value $\varphi = \pi$ represents the best fitting parameter to reproduce the experimental finding of sub-gap dips in the N/S junction under discussion. The temperature evolution of the conductance spectra within the two models shows a different behavior of the ZBC and E_{dip}. By rising the temperature, a non-monotonic evolution of E_{dip} (Fig. 3.2(c)) and a faster reduction of ZBC (Fig. 3.2(d)) is observed for the case of Fig. 3.2(b). As a

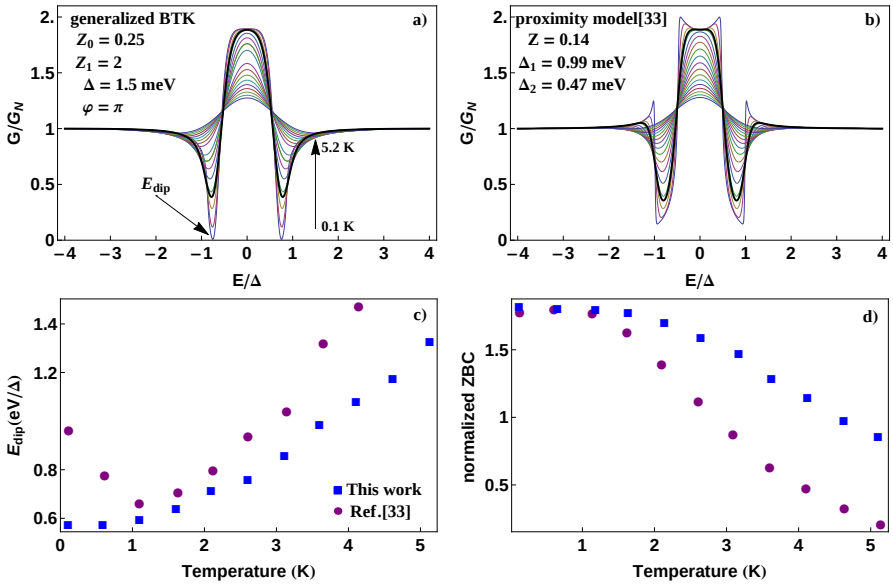

Figure 3.2: Temperature evolution of the normalized conductance curves obtained for (a) generalized BTK model with particle-hole mixing boundary conditions and for (b) proximity model[33] for the parameters $Z = 0.14$, $\Delta_1 = 0.99meV$ (bulk gap), $\Delta_2 = 0.47meV$ (proximized gap). The thick black line in the two plots represent the best fit for Cu/Nb experimental data reported in Ref.[33]. (c) Comparison of the temperature evolution of the energy position of the conductance dips, E_{dip} vs T, obtained from (a) and (b). (d) Comparison of the temperature evolution of the ZBC, obtained from (a) and (b).

consequence, very low temperature experiments are necessary to distinguish the two models and for understanding the physical origin of the anomalous conductance features observed in the point contact experiments in N/S devices. It is worth noticing that both models are physically plausible. Indeed, Nb and Cu oxides are known to exhibit magnetic correlations that could realize effective local polarization enabling a phase shift of π at the interface; on the other hand, the formation of a (proximized) weak superconducting layer at the N/S interface (proximity model) is also possible.

3.6 Discretized model

In order to identify the physical conditions for the presence of dips in the conductance curves (*see* Figs. 3.1 and 3.2) that can be associated to a localized polarization at the interface, we consider a discretized formulation that allows to describe spatial dependent potentials without increasing the computation complexity. We model a system with an odd number of sites N in which $(N-1)/2$ sites are used for both the normal and the superconducting side, while one normal site with magnetic (Γ) and non-magnetic potential (U) is considered at the interface (see Fig. 3.3). The nearest-neighbor hopping

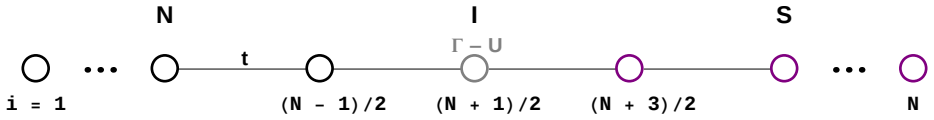

Figure 3.3: Discretized model of the N/S junction consisting of N (odd) sites: $(N+1)/2$ normal (N) sites; magnetic (Γ) and non-magnetic (U) potential are present at the interface (I) site $i=(N+1)/2$. The hopping parameter t is homogeneous along the system.

parameter t is assumed homogeneous and it is used as energy unit, $t \simeq 10\Delta_{Nb}$ in order to have $\xi_{Nb} \simeq 10a$. Temperature is measured in dimensions units $\tau = k_B T/t$. The transparency of the interface is controlled by the on-site potential U or equivalently can be controlled coupling the magnetic impurity to the normal and superconducting side with different hopping values. The BdG equations that we have to discretize are

$$\begin{pmatrix} -\frac{\hbar^2}{2m}\partial_x^2 + (U+\sigma\Gamma)\,\delta(x) & \sigma\Delta(x) \\ \sigma\Delta^*(x) & \frac{\hbar^2}{2m}\partial_x^2 - (U+\sigma\Gamma)\,\delta(x) \end{pmatrix} \psi^\sigma(x) = E\psi^\sigma(x) \quad (3.13)$$

where $\sigma = \pm$, with $\pm = \uparrow / \downarrow$ and $\psi^\sigma(x) = (u_\sigma, v_{\bar{\sigma}})^t$ is the BdG state in the absence of spin-flip associate with energy E. Using the discretized version

for the second derivative

$$\partial_x^2 \psi^\sigma(x) = \frac{\psi^\sigma(x-a) - 2\psi^\sigma(x) + \psi^\sigma(x+a)}{a^2}, \tag{3.14}$$

and the discretized BdG state $\psi_i^{(\sigma)} = (u_{\sigma,i}, v_{\bar{\sigma},i})^t$ $(\forall i \in [1, N])$, we can write:

$$\begin{aligned} -\frac{\hbar^2}{2m}\partial_x^2 u_{\sigma,i} &= -\frac{\hbar^2}{2ma^2}u_{\sigma,i-1} + \frac{\hbar^2}{ma^2}u_{\sigma,i} - \frac{\hbar^2}{2ma^2}u_{\sigma,i+1} \\ \frac{\hbar^2}{2m}\partial_x^2 v_{\bar{\sigma},i} &= \frac{\hbar^2}{2ma^2}v_{\bar{\sigma},i-1} - \frac{\hbar^2}{ma^2}v_{\bar{\sigma},i} + \frac{\hbar^2}{2ma^2}v_{\bar{\sigma},i+1}. \end{aligned} \tag{3.15}$$

Evaluating the other quantities in $x = ia$ we have

$$\begin{aligned} (U + \sigma\Gamma)\,\delta(x) &= (U + \sigma\Gamma)\,\delta_{i,(N+1)/2} \\ \sigma\Delta(x) &= \sigma\Delta_i. \end{aligned} \tag{3.16}$$

Finally, by expressing the nearest-neighbor parameter in terms of the sites distance a, $t = \hbar^2/(2ma^2)$ and by introducing the energy of the i-th lattice site $\varepsilon_i/t = 2 + U\delta_{i,(N+1)/2}$

$$\begin{aligned} &\left(\varepsilon_i + \sigma\Gamma\delta_{i,(N+1)/2} - E\right) u_{\sigma,i} - t\left(u_{\sigma,i-1} + u_{\sigma,i+1}\right) + \sigma\Delta_i v_{\bar{\sigma},i} = 0 \\ &\left(-\varepsilon_i - \sigma\Gamma\delta_{i,(N+1)/2} - E\right) v_{\bar{\sigma},i} + t\left(v_{\bar{\sigma},i-1} + v_{\bar{\sigma},i+1}\right) + \sigma\Delta_i^* u_{\sigma,i} = 0. \end{aligned} \tag{3.17}$$

The discretized version of BdG equations, then, can be written as

$$\mathcal{M}_i^{(\sigma)}\psi_i^{(\sigma)} + T\left(\psi_{i+1}^{(\sigma)} + \psi_{i-1}^{(\sigma)}\right) = 0, \tag{3.18}$$

where

$$\mathcal{M}_i^{(\sigma)} = \begin{pmatrix} \varepsilon_i - E + \sigma\Gamma_i & \sigma\Delta_i \\ \sigma\Delta_i^* & -\varepsilon_i - E + \sigma\Gamma_i \end{pmatrix}, \tag{3.19}$$

while $T = -t\hat{\sigma}_z$. Here $\Gamma_i/t = \Gamma\delta_{i,(N+1)/2}$ is the site-dependent Zeeman energy that we take different from zero only at the interface site. Using the boundary conditions $\psi_1^{(\sigma)} = \psi_N^{(\sigma)} = 0$, we get electron-like eigenstates

$$\Phi^{(\sigma,n)} = \sum_{i=1}^{N} (\delta_{1,i}, \ldots, \delta_{N,i})^t \otimes \left(u_{\sigma,i}^{(n)}, v_{\bar{\sigma},i}^{(n)}\right)^t \tag{3.20}$$

associated to positive eigenvalues $(\epsilon_n \geq 0)$. Now we let us compute the spatial dependence of the superconducting gap. The energy gap is given by:

$$\Delta(x) = \lambda(x)\,\langle\psi_\downarrow(x)\,\psi_\uparrow(x)\rangle. \tag{3.21}$$

We express the field operators in terms of Bogoliubov transformation

$$\psi_\sigma(x) = \sum_n \left[u_{n\sigma}(x)\,\gamma_n + v^*_{n\sigma}(x)\,\gamma^\dagger_n\right], \tag{3.22}$$

from which follows

$$\begin{aligned}\Delta(x) &= \lambda(x)\sum_{n,m}\left[\langle\left(u_{n\downarrow}(x)\,\gamma_n + v^*_{n\downarrow}(x)\,\gamma^\dagger_n\right)\left(u_{m\uparrow}(x)\,\gamma_m + v^*_{m\uparrow}(x)\,\gamma^\dagger_m\right)\rangle\right] \\ &= \lambda(x)\sum_{n,m}\left[u_{n\downarrow}(x)\,u_{m\uparrow}(x)\,\langle\gamma_n\gamma_m\rangle + u_{n\downarrow}(x)\,v^*_{m\uparrow}(x)\,\langle\gamma_n\gamma^\dagger_m\rangle\right. \\ &+ \left. v^*_{n\downarrow}(x)\,u_{m\uparrow}(x)\,\langle\gamma^\dagger_n\gamma_m\rangle + v^*_{n\downarrow}(x)\,v^*_{m\uparrow}(x)\,\langle\gamma^\dagger_n\gamma^\dagger_m\rangle\right].\end{aligned} \tag{3.23}$$

Here the symbol $\langle\ldots\rangle$ denotes a thermal average. By substituting $\langle\gamma_m\gamma_m\rangle = \langle\gamma^\dagger_m\gamma^\dagger_m\rangle = 0$, $\langle\gamma^\dagger_n\gamma_m\rangle = \delta_{nm}f(\epsilon_n)$, $\langle\gamma_n\gamma^\dagger_m\rangle = \delta_{nm}(1-f(\epsilon_n))$, where $f(\epsilon_n) = 1/\left[e^{\beta\epsilon_n}+1\right]$ is the Fermi-Dirac distribution, and using the symmetry relations for the coherence factors[19], we have

$$\Delta(x) = \frac{\lambda(x)}{2}\sum_n\left[u_{n\uparrow}(x)\,v^*_{n\downarrow}(x) - u_{n\downarrow}(x)\,v^*_{n\uparrow}(x)\right]\tanh\left(\frac{\epsilon_n}{2k_BT}\right), \tag{3.24}$$

that evaluated at $x = ia$ gives

$$\Delta_i = \frac{\lambda_i}{2}\sum_n\left[u^{(n)}_{\uparrow,i}v^{(n)*}_{\downarrow,i} - u^{(n)}_{\downarrow,i}v^{(n)*}_{\uparrow,i}\right]\tanh\left(\frac{\epsilon_n}{2k_BT}\right), \tag{3.25}$$

where the sum is calculated for $\epsilon_n \in [0, \hbar\omega_D]$, being $\hbar\omega_D$ the Debye energy. The attractive phonon-mediated local potential λ_i is assumed constant ($\lambda_i = \lambda$) also in the normal side of the junction to take into account proximity effects. Note that the numerical results do not change taking $\lambda_i = \lambda \neq 0$ only in the S-region and in the proximized N-region whose extension is about $\xi \sim 10a$. We consider the bulk superconducting gap Δ_{bulk} at the center of the S-region, in order to avoid finite size effects. Δ_{bulk} is computed self-consistently using Eq. (3.25) with accuracy better than 1% starting from $\Delta_i = 0.15t$ in S and by fixing $\lambda = 2.4t$. The polarizing effect of the magnetic site at the interface can be quantified by the site-dependent polarization

$$P_i = \frac{n_{i,\uparrow} - n_{i,\downarrow}}{n_{i,\uparrow} + n_{i,\downarrow}}, \tag{3.26}$$

where

$$\begin{aligned}n_{i,\uparrow} - n_{i,\downarrow} &= \sum_n\left[|u^{(n)}_{\uparrow,i}|^2 f(\epsilon_n) - |v^{(n)}_{\downarrow,i}|^2(1-f(\epsilon_n))\right] \\ &+ \sum_n\left[-|u^{(n)}_{\downarrow,i}|^2 f(\epsilon_n) + |v^{(n)}_{\uparrow,i}|^2(1-f(\epsilon_n))\right]\end{aligned} \tag{3.27}$$

and

$$\begin{aligned} n_{i,\uparrow} + n_{i,\downarrow} &= \sum_n \left[|u^{(n)}_{\uparrow,i}|^2 f(\epsilon_n) + |v^{(n)}_{\downarrow,i}|^2 (1 - f(\epsilon_n)) \right] \\ &+ \sum_n \left[|u^{(n)}_{\downarrow,i}|^2 f(\epsilon_n) + |v^{(n)}_{\uparrow,i}|^2 (1 - f(\epsilon_n)) \right]. \end{aligned} \tag{3.28}$$

Eqs. (3.27) and (3.28) were obtained in the same fashion as the superconducting energy gap. We set $t = 16.2\, meV$ as the energy cut-off, that is of the same order of magnitude of the Debye energy, in agreement with the choice that only states with phonon-mediated attraction are retained. In order to capture the bulk-like behaviour using a finite size system, the system size N has been progressively increased from $N = 15$ to $N = 71$, while monitoring the temperature dependence of Δ_{bulk}. The results of this analysis are shown in Figure 3.4(a) where normalized values of Δ_{bulk} are presented as a function of the dimensionless temperature τ. For a system size of $N = 15$ a size-induced suppression of the superconducting gap is observed, this effect being more evident close to the transition temperature τ_c. Increasing the system size up to $N = 51$ produces a Δ_{bulk} vs τ curve very close to the one obtained for the $N = 71$ case, signaling that the bulk limit of the interface model has been reached. The temperature evolution of Δ_{bulk} for $N = 71$ has been compared with the BCS behaviour giving a dimensionless critical temperature $\tau_c = 0.0485$, corresponding to a niobium critical temperature $T_c^{Nb} \simeq 9.1K$. In Figure 3.4(b) we present the spatial dependence of the superconducting gap (for system size $N = 51$ and $N = 71$) fixing the Zeeman energy Γ of the magnetic potential in the range $[-2.5, 0]$, while taking $U = 0$ (transparent interface) and $\tau = 0.025$ (i.e. $T \sim T_c^{Nb}/2$). In order to compare spectra obtained for systems with different size, the data referring to $N = 51$ have been rescaled. For $-1.0 < \Gamma < 0$ we observe ordinary proximity effect where finite superconducting order parameter is induced in the N-side on a length of about $10a \simeq \xi_{Nb}$. For sufficiently strong magnetization $\Gamma \leq -1.0$ negative order parameter is induced on the same length scale. Reduction of the order parameter on the right border is due to the S/vacuum interface. In Figure 3.4(c) we show the spatial dependence of the polarization, calculated for $\Gamma \in [-2.5, 0]$ and $U = 0$. The polarizing effect of the localized magnetic moment asymmetrically extends on a distance of about $20a$. In the superconducting side the induced polarization is inverted for large Γ values[56] ($\Gamma < -2.0$). The general aspect of the polarization curves evidences Friedel density oscillations. We have also verified the effect of barrier strength on the inversion of the superconducting order parameter. In Figure 3.4(d), we show the gap value calculated (at site $i = 25$) in proximity of the interface, for a system size $N = 51$, as a function of Γ, with enhanced resolution (step 0.1).

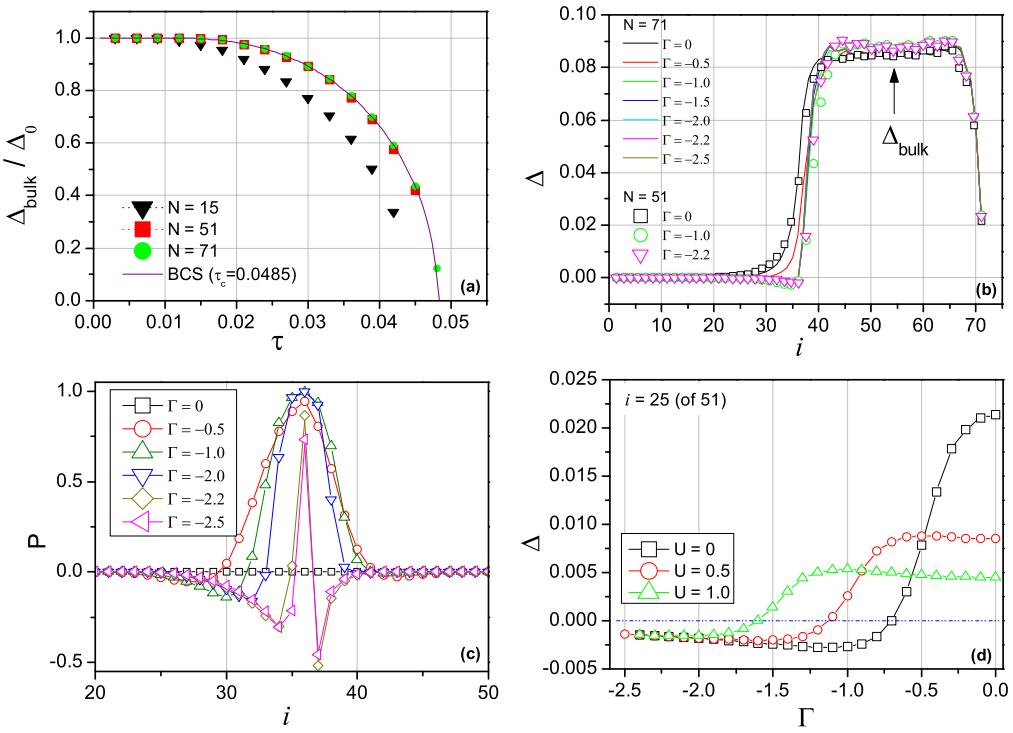

Figure 3.4: Numerical results obtained in the discretized model. (a) Temperature dependence of the bulk superconducting gap for different systems, namely $N = 15$, $N = 51$, $N = 71$, assuming transparent barrier, $U = 0$. Numerical data, normalized to the low temperature value Δ_0, are compared to theoretical behaviour expected in the BCS model for $\tau_c = 0.0485$. (b) Spatial dependence of the superconducting gap for 71-sites and 51-sites systems, by assuming $U = 0$, a constant BCS coupling, $\lambda_i = \lambda$, and dimensionless temperature $\tau = 0.025$. Different curves correspond to different values of Γ. Lines refer to data obtained for 71-sites system; scattered symbols refer to 51-sites system, rescaled to compare the data sets. The arrow indicates the region where the superconducting gap is calculated self-consistently. (c) Spatial dependence of the polarization calculated for $N = 71$ for different Γ values, with $U = 0$ and $\tau = 0.025$. (d) Effect of the barrier strength U: the superconducting gap vs Γ is evaluated at the site $i = 25$ (of 51), at $\tau = 0.025$ for three different transparency conditions ($U = 0$, $U = 0.5$, $U = 1$), the magnetic site being located at $i = 26$.

For reduced transparency ($U > 0$) a larger magnetic moment is necessary to induce the inversion of the interface order parameter. The analysis of the pairing potential Δ_i shows that, in presence of a local polarization at the interface, a phase gradient $\varphi = \pi$ can be stabilized. For relatively transparent junctions (i.e. described by small values of U) the sign change of the interface order parameter can be obtained with moderate polarization strength, while strong polarization values are needed for opaque interface with higher values of U. Thus the probability to observe an hidden magnetic moment at the interface accompanied by a phase gradient is enhanced in transparent systems. The physical origin of a local magnetic moment at the Cu/Nb interface probably resides in many-body effects which can be accounted for in the framework of the Anderson impurity model[57].

3.7 Physical meaning of particle-hole mixing parameter

In this section we discuss the range of variability of the particle-hole mixing interface potential Z_1 that we have added to the standard BTK theory and the validity of the generalized BTK model. The off-diagonal potential mimicking the proximity effect is given by:

$$V^{eh}(x) = U_1 \begin{pmatrix} 0 & i\hat{\sigma}_y e^{i\varphi} \\ -i\hat{\sigma}_y e^{-i\varphi} & 0 \end{pmatrix} \delta(x). \tag{3.29}$$

We would like to connect the phenomenological parameter U_1 to the microscopic parameters of the junction. Requiring that the spatial average of $V^{eh}(x)$ over the proximized normal region, i.e. $x \in [-\xi, 0^+]$, is related to the average pairing $|\bar{\Delta}|$ experienced by the particles at the interface, we get the equation:

$$\xi^{-1} \int_{-\xi}^{0^+} V^{eh}(x)\, dx = |\bar{\Delta}| \begin{pmatrix} 0 & i\hat{\sigma}_y e^{i\varphi} \\ -i\hat{\sigma}_y e^{-i\varphi} & 0 \end{pmatrix}. \tag{3.30}$$

Solving Eq. (3.30), we obtain $U_1 = \xi|\bar{\Delta}|$, with $|\bar{\Delta}| > 0$. From the above arguments we can write $Z_1 = 2m\xi|\bar{\Delta}|/\hbar^2 k_F = \xi|\bar{\Delta}|k_F/E_F$. Moreover, recalling the expression of the coherence length $\xi \approx \hbar v_F/2\Delta_{bulk}$, the mixing strength Z_1 can be represented in the form of ratio $Z_1 = |\bar{\Delta}|/\Delta_{bulk}$. Assuming that $|\bar{\Delta}|$ is just a fraction of the bulk pairing potential Δ_{bulk}, one expects small mixing strength. However its value is increased in the presence of band bending effects due to charge transfers and orbital reconstruction which can significally modify the quasiparticle effective mass m, the Fermi

energy E_F and the particles velocity v_F at the interface. E.g. for niobium-based interface characterized by $k_F\xi \approx 400$ ($\xi_{Nb} \approx 40nm, k^{-1}_{F,Nb} \sim 0.1nm$) and $|\bar{\Delta}| \approx 0.5meV$ ($0.3\Delta_{bulk}$), using $Z_1 = \xi|\bar{\Delta}|k_F/E_F$, we get $Z_1 = 0.2/E_F$, the Fermi energy being measured in eV. Since in nanostructured systems (thin films) E_F can take values significantly lower than $1eV$, we can conclude that Z_1 can be of the order and greater than 1 (e.g. $Z_1 \simeq 1.3$ for $E_F = 0.15eV$). Values of $Z_1 \simeq 2$ can be reached considering $|\bar{\Delta}| \approx 0.5\Delta_{bulk}$ and $E_F = 0.15eV$. This simple argument justifies the values of Z_1 greater than unity used in Fig. 3.1. However a better insight on the role of Z_1 can be inferred by studying the conductance in a $NS'S$ model, where S is the bulk superconductor and S' is the superconducting proximity region of length $d \sim \xi$ with a gap modulus $\Delta' < \Delta_{bulk}$. The N/S' interface is assumed to be transparent, while the opacity of S'/S interface is controlled by the barrier strength Z. Calculating the Andreev reflection and normal reflection coefficients by using the usual BTK boundary condition of the scattering wave function at the N/S' interface and S'/S interface, we can evaluate the zero temperature differential conductance for a phase difference between S and S', $\varphi = 0$ or π. The results are reported in Fig.3.5 where the zero temperature

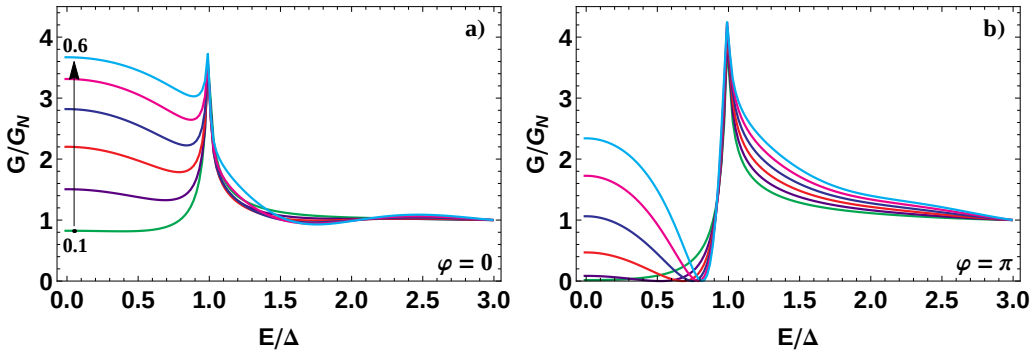

Figure 3.5: Zero temperature conductance curves obtained in the NS′S model as a function of ϵ/Δ. Different curves in both panels are obtained fixing the ratio $\Delta'/\Delta_{bulk} = 0.1$ (lowest curve), 0.2, 0.3, 0.4, 0.5, 0.6 (highest curve). The remaining parameters are $Z = 2.5$, $k_Fd = 380$ and $\varphi = 0$ (left panel) or $\varphi = \pi$ (right panel).

conductance G/G_N is plotted as a function of E/Δ. The different curves are obtained at varying the ratio Δ'/Δ_{bulk} (0.1 to 0.6 from below), while fixing the remaining parameters as $Z = 2.5$, $k_Fd = 380$ (of the order of the coherence length $k_F\xi = 400$) and $\varphi = 0$ (left panel) or $\varphi = \pi$ (right panel). Here it is shown that zero conductance dips within the gap are obtained for $\varphi = \pi$ and an high value of Z (right panel of Fig.3.5). This indicates that

the role of Z_1 in the generalized BTK model is similar to that of the ratio Δ'/Δ_{bulk} in the $NS'S$ model under the assumption of low-transparency of the S'/S interface. This is confirmed observing that the dip-peak structure in Fig. 3.1 (right column) appears as Z_1 is increased ($Z_1 > 1$). The same effect is obtained in the $NS'S$ model by increasing Δ'/Δ_{bulk} in the presence of low-transparency of the barrier (high value of Z). This suggests that the parameter Z_1 not only retains information on the proximity effect but also contributes to renormalize the interface transparency producing a more opaque local potential. The comparison between the generalized BTK model and the $NS'S$ model shows that the dip-peak structure in the conductance is not an artifact of the delta-like form of the particle-hole mixing potential but it is related to a genuine proximity effect, which can also be studied in the framework of an $NS'S$ model setting high Z values (tunnel limit) and moderate Δ'/Δ_{bulk} ratio. Let us finally note that the $NS'S$ model we have considered here, differs from the proximity model[33] where the results for the conductance do not depend on the proximity region length d and on the relative superconducting phase φ.

In summary, we have generalized the BTK theory, including particle-hole mixing boundary condictions in the scattering problem, that allows a complete parametrization of the interface effects in terms of three parameters, namely Z_0, Z_1 and φ. We have calculated the finite-temperature differential conductance spectra showing the formation of conductance dips in the case of a phase $\pi-$shift at the interface. This value for the phase can be explained in terms of a localized magnetic moment at the interface, that could make a sign change of the superconducting order parameter energetically favorable. We have demonstrated that the generalized BTK model reproduce the experimental data reported for Cu/Nb contacts in Ref.[33] and we have discriminate the physical origin of the conductance dips through a temperature evolution of the conductance spectra. Finally, we have used a tight-binding model to determine the necessary physical conditions under which the π-shift is realized: transparent interfaces can easily sustain a phase gradient as the effect of a weak interface magnetization, while for reduced transparencies a relative strong localized magnetization would be necessary.

Chapter 4

Spin-orbit interaction effects at the interface

In this chapter we study the spin transport in an N/S junction in the presence of Rashba spin-orbit coupling at the interface. Our aim is to analyze to what extend superconducting junctions can be employed for spintronics purpose. One of the fundamental goal of the spintronics is to create, detect and control the spin current, that represents a key part in the understanding phenomena such as the giant magnetoresistance effect (GMR)[58, 59]. An important aspect of the spintronics research includes the control of spin relaxation, that is the ability to make that electron remembers its spin polarization along the required paths. If spin relaxes too fast, the distance traversed by electron without losing its spin will be too short to serve any pratical purpose. If the electron spin would be decoupled from the orbital motion, the only possibility to influence it could be provided by an external magnetic field. The most important interaction which causes spin relaxation is spin-orbit (SO) interaction, which couples an electron's spin degree of freedom to its orbital motion. This makes the SO interaction to be the key ingredient for the spin control and relaxation and motivates the studies of SO coupling in different systems[60, 61]. In particular two-dimensional electron gas (2DEG) is considered as the basic system for these studies since properties of other nanosystems such as quantum wires and quantum dots, are directly related to or derived from the properties of the 2DEG. It has been shown that the confining potential along the vertical direction causes the structure inversion asymmetry from which results an effective SO interaction known as Rashba spin-orbit coupling (RSOC)[62, 63]. As a result, RSOC is controllable via an applied electric field[64], thus providing a convenient method of spin control[65]. Motivated by the advantages of RSOC in spintronics[65], the influences of the RSOC on the Andreev reflec-

tion (AR) have been studied[66, 67, 68, 69]. In particular, Linder *et al.*[70] have demonstrated that a spin current may arise in hybrid structures when spin-orbit interaction is present at the interface. This stems from the broken inversion symmetry near the interface which induces an electric field perpendicular to it, allowing for the spin-flip at the interface. Furthermore, a RSOC at the interface can be a source for a triplet superconducting proximity effect[71, 72, 73, 74] because it provides a spin-dependent potential. Thus understanding the role of spin-orbit coupling at the interface is relevant for both superconducting and transport properties.

4.1 Origin of spin-orbit interaction

Spin-orbit (SO) interaction is a well-known phenomen that manifests itself in lifting the degeneracy of one-electron energy levels[80]. It is a relativistic correction to the Schrödinger equation, which arises as a combination of two effects: (i) the effective magnetic field experienced in its rest frame by an electron moving in an electric field and (ii) the Thomas precession of the rest frame of an accelerated electron. We can derive and understand the existence of this interaction in the following fashion. Consider an electron orbiting around the nucleus; from the rest frame of the electron the nucleus is circling around it with velocity $\boldsymbol{v}$, then feels an effective magnetic field given by

$$\boldsymbol{B} = \frac{\boldsymbol{v}}{c} \times \boldsymbol{E}, \tag{4.1}$$

where $\boldsymbol{E}$ is the electric field due to the nucleus. The magnetic momentum of the electron $\boldsymbol{\mu}$ and the spin angular momentum $\boldsymbol{S}$ are related by

$$\boldsymbol{\mu} = \frac{eg}{2mc}\boldsymbol{S}, \tag{4.2}$$

where the factor g has the value $g = 2$. Then the equation of motion for its spin angular momentum in its rest frame is

$$\left(\frac{d\boldsymbol{S}}{dt}\right)_{restframe} = \boldsymbol{\mu} \times \boldsymbol{B}'. \tag{4.3}$$

Here

$$\boldsymbol{B}' = \gamma\left(\boldsymbol{B} - \frac{\boldsymbol{v}}{c} \times \boldsymbol{E}\right) \tag{4.4}$$

is the magnetic field in that frame, with $\boldsymbol{B}$ and $\boldsymbol{E}$, respectively, the magnetic and electric field in the nucleus rest frame. Then, neglecting terms of the

order of v^2/c^2 we have

$$\left(\frac{d\boldsymbol{S}}{dt}\right)_{restframe} = \boldsymbol{\mu} \times \left(\boldsymbol{B} - \frac{\boldsymbol{v}}{c} \times \boldsymbol{E}\right), \tag{4.5}$$

that is equivalent to an energy of interaction of the electron spin:

$$U' = -\boldsymbol{\mu} \cdot \left(\boldsymbol{B} - \frac{\boldsymbol{v}}{c} \times \boldsymbol{E}\right). \tag{4.6}$$

In case of centrally symmetric electric field the electric force $e\boldsymbol{E}$ is given by

$$\boldsymbol{E} = -\frac{1}{e}\frac{\boldsymbol{r}}{r}\frac{dV(\boldsymbol{r})}{dr}, \tag{4.7}$$

from which follows that the spin-interaction energy can be written as

$$U' = -\frac{eg}{2mc}\boldsymbol{S} \cdot \boldsymbol{B} + \frac{g}{2m^2c^2}\boldsymbol{S} \cdot \boldsymbol{L}\left(\frac{1}{r}\frac{dV(\boldsymbol{r})}{dr}\right), \tag{4.8}$$

where $\boldsymbol{L} = \boldsymbol{r} \times m\boldsymbol{v}$ is the orbital angular momentum of the electron. This interaction energy gives the anomalous Zeeman effect correctly, but has a spin-orbit interaction that is twice too large. There is an explanation for this due to a relativistic kinematic effect pointed out by Thomas. If the coordinate system rotate the equation of motion for spin (Eq. (4.3)) becomes

$$\left(\frac{d\boldsymbol{S}}{dt}\right)_{nonrot} = \left(\frac{d\boldsymbol{S}}{dt}\right)_{restframe} + \boldsymbol{\omega}_T \times \boldsymbol{S} = \boldsymbol{S} \times \left(\frac{eg\boldsymbol{B'}}{2mc} - \boldsymbol{\omega}_T\right). \tag{4.9}$$

The corresponding energy of interaction is

$$U = U' + \boldsymbol{S} \cdot \boldsymbol{\omega}_T, \tag{4.10}$$

where the Thomas angular velocity is given by

$$\boldsymbol{\omega}_T = -\frac{1}{2m^2c^2}\boldsymbol{L}\left(\frac{1}{r}\frac{dV(\boldsymbol{r})}{dr}\right). \tag{4.11}$$

Thus

$$U = -\frac{eg}{2mc}\boldsymbol{S} \cdot \boldsymbol{B} + \frac{(g-1)}{2m^2c^2}\boldsymbol{S} \cdot \boldsymbol{L}\frac{1}{r}\frac{dV(\boldsymbol{r})}{dr}. \tag{4.12}$$

With $g = 2$ the spin-orbit interaction (Eq. (4.8)) reduced by 1/2 (known as Thomas factor) as required for the correct result:

$$H_{SO} = \frac{1}{2m^2c^2}\boldsymbol{S} \cdot \boldsymbol{L}\frac{1}{r}\frac{dV(\boldsymbol{r})}{dr}. \tag{4.13}$$

The form of SO leads to a shift in the energy spectrum of the electron. To summarize, the essence of SO is that the moving electron in an electric field feels an effective magnetic field even without any external magnetic field.

4.2 Rashba spin-orbit coupling

The Kramers theorem[81] for time-reversal invariant systems requires that the energy of an electron satisfies $E(\boldsymbol{k},\uparrow) = E(-\boldsymbol{k},\downarrow)$, since $\boldsymbol{k} \to -\boldsymbol{k}$ and $\sigma \to -\sigma$ upon time-reversal, so that a state corresponding to spin-up a wave vector $\boldsymbol{k}$ is degenerate with spin-down state of wave vector $-\mathbf{k}$. SO preserves time-reversal symmetry. If in addition there is an inversion symmetry in the system the Kramers theorem gives degenerate spin states for any value of $\boldsymbol{k}$, $E(\boldsymbol{k},\uparrow) = E(\boldsymbol{k},\downarrow)$. Spin-splitting due to the structure inversion asymmetry is determined by Rashba spin-orbit coupling (RSOC)[62, 63] and is described by the following Hamiltonian:

$$\hat{H}_{SO} = \alpha(\boldsymbol{\sigma} \times \boldsymbol{k}) \cdot \hat{\boldsymbol{n}}, \tag{4.14}$$

where α is a parameter describing the strength of RSOC, $\boldsymbol{\sigma}$ is the vector of Pauli spin matrices and $\hat{\boldsymbol{n}}$ is a unit vector oriented along the axis to which the crystal has an high-symmetry. Due to the fact that in hybrid structures the materials that compose them have different electron density, electrons will redistribuite near the interface moving from one material to the other. This induces an electric field $\boldsymbol{E}$ perpendicular to the interface along the $\hat{\boldsymbol{n}}$ direction, where $\hat{\boldsymbol{n}}$ is an interface normal vector. This field breaks the $\hat{\boldsymbol{n}} \to -\hat{\boldsymbol{n}}$ symmetry and thus can generate a nonzero RSOC localized near the interface[68, 69, 70, 82, 83, 84]. The Rashba spin-orbit term can be interpreted as an interaction with an effective magnetic field

$$\mathbf{B}_{SO} \propto \boldsymbol{k} \times \hat{\boldsymbol{n}}, \tag{4.15}$$

since $(\boldsymbol{\sigma} \times \boldsymbol{k}) \cdot \hat{\boldsymbol{n}} = \boldsymbol{k} \cdot (\hat{\boldsymbol{n}} \times \boldsymbol{\sigma})$. RSOC can be tuned by an external gate voltage[64, 85, 86, 87]. In this work, we will investigate the effects of RSOC at the interface in N/S junctions.

4.3 Spin current and spin torque in hybrid structures

Let us consider a system, composed by a superconductor connected to a normal-metal, described by the following Hamiltonian in a four-component BdG formalism:

$$\mathcal{H} = \begin{pmatrix} H_0 + V(\mathbf{r},\boldsymbol{\sigma}) & \Delta(\mathbf{r}) \\ \Delta^{\dagger}(\mathbf{r}) & -(H_0 + V(\mathbf{r},\boldsymbol{\sigma}))^{*} \end{pmatrix}, \tag{4.16}$$

where H_0 is the kinetic operator defined by

$$H_0 = \left[-\frac{\hbar^2}{2m}\nabla^2 - E_F \right] \mathbb{I} \tag{4.17}$$

being E_F the Fermi energy and $\mathbb{I}$ the identity operator in the spin space, $V(\mathbf{r}, \boldsymbol{\sigma})$ is a spin-dependent potential, that may describe Zeeman or spin-orbit interaction and finally for an s-wave superconductor $\Delta(\mathbf{r}) = i\sigma_y \Delta(\mathbf{r})$, where σ_y is a Pauli matrix. In order to derive an expression of the spin current, we consider the spin operator density defined, at position $\mathbf{r}$ and time t as[75]

$$S^{\mu}(\mathbf{r}, t) = \psi^{\dagger}(\mathbf{r}, t) \frac{\hbar}{2} \sigma^{\mu} \psi(\mathbf{r}, t), \tag{4.18}$$

where $\sigma^{\mu} = \{\sigma^x, \sigma^y, \sigma^z\}$ are the Pauli matrices, $\psi(\mathbf{r}, t) = (u_{\uparrow}(\mathbf{r}, t), u_{\downarrow}(\mathbf{r}, t), v_{\uparrow}(\mathbf{r}, t), v_{\downarrow}(\mathbf{r}, t))^t$ is the wave function that describes the system. The equation of motion for $S^{\mu}(\mathbf{r}, t)$ is

$$\partial_t S^{\mu}(\mathbf{r}, t) = -\frac{i}{\hbar} \left[S^{\mu}(\mathbf{r}, t), \mathcal{H} \right]. \tag{4.19}$$

From the Schrödinger equation, we have $\overrightarrow{\mathcal{H}} \psi(\mathbf{r}, t) = i\hbar \partial_t \psi(\mathbf{r}, t)$ and $\psi^{\dagger}(\mathbf{r}, t) \overleftarrow{\mathcal{H}} = -i\hbar \partial_t \psi^{\dagger}(\mathbf{r}, t)$. By using the above two equations, Eq. (4.19) becomes

$$\partial_t S^{\mu}(\mathbf{r}, t) = \frac{1}{2i} \left\{ \psi^{\dagger}(\mathbf{r}, t) \sigma^{\mu} \overrightarrow{\mathcal{H}} \psi(\mathbf{r}, t) - \psi^{\dagger}(\mathbf{r}, t) \overleftarrow{\mathcal{H}} \sigma^{\mu} \psi(\mathbf{r}, t) \right\}. \tag{4.20}$$

By substituting the Hamiltonian (Eq. (4.16)) in Eq. (4.20) we obtain

$$\begin{aligned} \partial_t S^{\mu}(\mathbf{r}, t) = & -\frac{\hbar}{2} \nabla \cdot \left[\psi^{\dagger}(\mathbf{r}, t) \begin{pmatrix} \sigma^{\mu} \boldsymbol{v} & 0 \\ 0 & -\sigma^{\mu *} \boldsymbol{v} \end{pmatrix} \psi(\mathbf{r}, t) \right] \\ & + \frac{i}{2} \psi^{\dagger}(\mathbf{r}, t) \begin{pmatrix} [V(\mathbf{r}, \boldsymbol{\sigma}), \sigma^{\mu}] & 0 \\ 0 & [-(V(\mathbf{r}, \boldsymbol{\sigma}))^*, \sigma^{\mu *}] \end{pmatrix} \psi(\mathbf{r}, t), \end{aligned} \tag{4.21}$$

where $\boldsymbol{v} = i\hbar/2m \left(\overrightarrow{\nabla} - \overleftarrow{\nabla} \right)$ is the velocity operator. Introducing the spin current density $\mathbf{J}_s(\mathbf{r}, t)$[76] and the density of spin torque $\tau(\mathbf{r}, t)$[77, 78]

$$\mathbf{J}_s^{\mu}(\mathbf{r}, t) = \frac{\hbar}{2} \psi^{\dagger}(\mathbf{r}, t) \begin{pmatrix} \sigma^{\mu} \boldsymbol{v} & 0 \\ 0 & -\sigma^{\mu *} \boldsymbol{v} \end{pmatrix} \psi(\mathbf{r}, t), \tag{4.22}$$

$$\tau^{\mu}(\mathbf{r}, t) = \frac{i}{2} \psi^{\dagger}(\mathbf{r}, t) \begin{pmatrix} [V(\mathbf{r}, \boldsymbol{\sigma}), \sigma^{\mu}] & 0 \\ 0 & [-(V(\mathbf{r}, \boldsymbol{\sigma}))^*, \sigma^{\mu *}] \end{pmatrix} \psi(\mathbf{r}, t), \tag{4.23}$$

then Eq. (4.21) reduces to

$$\partial_t S^\mu (\mathbf{r}, t) = -\nabla \cdot \mathbf{J}_s^\mu (\mathbf{r}, t) + \tau^\mu (\mathbf{r}, t) . \tag{4.24}$$

The spin current does not conserve giving rise to a source term $\tau^\mu (\mathbf{r}, t)$ that corresponds to the torsion of the spin. When $[V (\mathbf{r}, \boldsymbol{\sigma}) , \boldsymbol{\sigma}] = 0$ the spin torque term vanishes and a continuity equation is obeyed by the spin current

$$\partial_t S^\mu (\mathbf{r}, t) + \nabla \cdot \mathbf{J}_s^\mu (\mathbf{r}, t) = 0. \tag{4.25}$$

In order to evaluate the spin torque we consider Eq. (4.24) under stationary conditions

$$\nabla \cdot \mathbf{J}_s^\mu (\mathbf{r}) = \tau^\mu (\mathbf{r}) . \tag{4.26}$$

In the case of a system in which we model the potential at the interface with a spin-dependent potential the spin torque can be calculated by integrating integral Eq. (4.26) from $-\epsilon$ to ϵ and then letting the limit for $\epsilon \to 0$

$$\hat{\boldsymbol{n}} \cdot (\mathbf{J}_{sR}^\mu (0) - \mathbf{J}_{sL}^\mu (0)) = \tau^\mu (0) , \tag{4.27}$$

where $\mathbf{J}_{sL/R}^\mu (0)$ and $\tau^\mu (0)$ are, respectively, the value of the spin current and of the spin torque at the interface and $\hat{\boldsymbol{n}}$ is the unit vector along the normal at the interface[79]. Since spin supercurrent can be present in junctions with spin-flip scattering at the interface and/or triplet superconductors, in the following, we will consider an interfacial spin-dependent potential and we will focus on the existence of the spin supercurrent in a N/S junction.

4.4 Model

Let us consider a three-dimensional N/S junction separated by an interface at $x = 0$. We assume that the Fermi energy E_F and the effective mass m in the normal metal ($x < 0$) are equal to those in the superconductor ($x > 0$) and $\boldsymbol{k} = k_F (\cos\theta \sin\phi, \sin\theta \sin\phi, \cos\phi)$ is the wave vector direction on the N and S side. The system is described by Bogoliubov-de Gennes equations [19]

$$[\mathcal{H} + V (\mathbf{r})] \psi (\mathbf{r}) = E\psi (\mathbf{r}) , \tag{4.28}$$

where E is the energy of a quasiparticle measured from E_F, $\psi (\mathbf{r}) = (u_\uparrow (\mathbf{r}) , u_\downarrow (\mathbf{r}) , v_\uparrow (\mathbf{r}) , v_\downarrow (\mathbf{r}))^t$ is a four-component wave function in the Nambu space, $\mathcal{H}$ is the Hamiltonian given by

$$\mathcal{H} = \begin{pmatrix} \hat{H}_0 (\mathbf{r}) & \hat{\Delta} (\mathbf{r}) \\ \hat{\Delta}^\dagger (\mathbf{r}) & -\hat{H}_0^* (\mathbf{r}) \end{pmatrix} \tag{4.29}$$

and $\hat{\Delta}(\mathbf{r})$ is the pairing potential. Specifically, $\hat{H}_0(\mathbf{r})$ is the single-particle Hamiltonian operator defined by

$$\hat{H}_0(\mathbf{r}) = \left[-\frac{\hbar^2}{2m}\nabla^2 - E_F\right]\hat{\mathbb{I}}, \tag{4.30}$$

with $\hat{\mathbb{I}}$ the identity operator in the spin space, while the barrier potential at the interface $V(\mathbf{r})$ is modelled as

$$V(\mathbf{r}) = \begin{pmatrix} U_0\hat{\mathbb{I}} + U_{soc} & U_t \\ U_t^{\dagger} & -U_0\hat{\mathbb{I}} - U_{soc}^{*} \end{pmatrix}\delta(x), \tag{4.31}$$

where $U_{soc} = U_{soc}\hat{\boldsymbol{n}}\cdot(\hat{\boldsymbol{\sigma}}\times\hat{\boldsymbol{p}})/p_F$, due to the presence at the interface of RSOC, with $\hat{\boldsymbol{n}} \equiv \hat{\boldsymbol{x}}$ the interface normal unit vector, $\hat{\boldsymbol{\sigma}}$ the Pauli matrices and $\hat{\boldsymbol{p}} = -i\hbar\boldsymbol{\nabla}$ the momentum operator, $U_t = i(\boldsymbol{d}(r)\cdot\hat{\boldsymbol{\sigma}})\hat{\sigma}_y$ is triplet pairing due to U_{soc} that allows spin-flip at the interface, where $\boldsymbol{d}(r)$ is the vector order parameter, orthogonal to the spin of the Cooper pairs, that assume the form $\boldsymbol{d}(r) = \tilde{U}\hat{\boldsymbol{x}}$ and $\tilde{U}$ is an operator, which for Cooper pairs in a relative $p-wave$ orbital state has the real space form $\tilde{U} = (U_t/\hbar k_F)\,\hat{\boldsymbol{u}}\cdot\hat{\boldsymbol{p}}$. The unit vector $\hat{\boldsymbol{u}}$ defines the orbital state: $\hat{\boldsymbol{u}} = \hat{\boldsymbol{z}}$ for $p_z - wave$ and $\hat{\boldsymbol{u}} = \hat{\boldsymbol{z}} + i\hat{\boldsymbol{y}}$ for $p_z + ip_y - wave$. In the following, it is convenient to express U_t in terms of the Fourier transform of $\tilde{U}$, which is written $U_k = (U_t/k_F)\,\hat{\boldsymbol{u}}\cdot\boldsymbol{k}$ and we consider the orbital pairing state: $p_y + ip_z - wave$, $U_t = (U_t/k_F)(k_y + ik_z)$. Here U_0 and U_{soc} are the strengths of the usual BTK and RSOC contributions, while the term U_t indicate the barrier strength due to the triplet pairing induced by RSOC. Finally for an s-wave superconductor, $\hat{\Delta}(\mathbf{r}) = i\hat{\sigma}_y\Delta(\mathbf{r})$ where $\hat{\sigma}_y$ is a Pauli matrix. We neglect for simplicity the self-consistency of spatial distribution of the pair potential in S and take it as a step function $\Delta(\mathbf{r}) = \Delta\theta(x)$, where Δ is the bulk superconducting gap and $\theta(x)$ is the Heaviside step function. Translational invariance along the $\hat{\boldsymbol{y}}$ and $\hat{\boldsymbol{z}}$ direction implies conservation of the momentum parallel to the interface $\mathbf{k}_{\parallel} = (0, k_y, k_z)$ and the solution of Eq. (4.28) takes the form $\psi(\mathbf{r}) = \psi(x)\,e^{i(k_y y + k_z z)}$, leading to an effective one-dimensional problem for $\psi(x)$.

4.5 Solutions of Bogoliubov-de Gennes equations

For an electron with spin $\sigma = \{\uparrow, \downarrow\}$ injected from the N side, with incidence angles (θ, ϕ) we have

$$\psi_N^{\sigma}(x) = \begin{pmatrix} \delta_{\uparrow\sigma} \\ \delta_{\downarrow\sigma} \\ 0 \\ 0 \end{pmatrix} e^{ik_x x} + \begin{pmatrix} r_e^{\sigma,\uparrow} \\ r_e^{\sigma,\downarrow} \\ 0 \\ 0 \end{pmatrix} e^{-ik_x x} + \begin{pmatrix} 0 \\ 0 \\ r_h^{\sigma,\uparrow} \\ r_h^{\sigma,\downarrow} \end{pmatrix} e^{iq_x x}, \tag{4.32}$$

where $k_x = k\cos\theta\sin\phi$, $q_x = q\cos\theta_A\sin\phi_A$, with $\hbar k = \sqrt{2m\left(E_F + E\right)}$ and $\hbar q = \sqrt{2m\left(E_F - E\right)}$ are the electron and hole wave vectors and (θ_A, ϕ_A) Andreev reflection angles. The coefficients $r_e^{\sigma,\nu}$ and $r_h^{\sigma,\nu}$, with $\nu = \{\uparrow, \downarrow\}$, represent the normal reflection and Andreev reflection, respectively. In the S side we have

$$\begin{aligned} \psi_S(x) &= t_e^{\sigma,\uparrow} \begin{pmatrix} u \\ 0 \\ 0 \\ v \end{pmatrix} e^{ik_{+x}x} + t_e^{\sigma,\downarrow} \begin{pmatrix} 0 \\ u \\ -v \\ 0 \end{pmatrix} e^{ik_{+x}x} \\ &+ t_h^{\sigma,\downarrow} \begin{pmatrix} v \\ 0 \\ 0 \\ u \end{pmatrix} e^{-ik_{-x}x} + t_h^{\sigma,\uparrow} \begin{pmatrix} 0 \\ v \\ -u \\ 0 \end{pmatrix} e^{-ik_{-x}x}, \end{aligned} \tag{4.33}$$

where $t_e^{\sigma,\uparrow}$, $t_e^{\sigma,\downarrow}$, $t_h^{\sigma,\uparrow}$ and $t_h^{\sigma,\downarrow}$ are the transmission coefficients of electron-like quasiparticle (ELQ) and hole-like quasiparticles (HLQ), while $k_{\pm x} = k_{\pm}\cos\theta_S\sin\phi_S$, with $\hbar k_{\pm} = \sqrt{2m\left(E_F \pm \sqrt{E^2 - \Delta^2}\right)}$, indicate ELQ and HLQ wave vectors and (θ_S, ϕ_S) are transmission angles, the BCS[14] coherence factors being

$$u^2 = 1 - v^2 = \frac{1}{2}\left(1 + \frac{\sqrt{E^2 - \Delta^2}}{E}\right). \tag{4.34}$$

As consequence, the wave function in the normal side is given by:

$$\psi_N\left(\mathbf{r}\right) = \psi_N^{\sigma}\left(x\right) e^{i(k_y y + k_z z)}, \tag{4.35}$$

while in the superconducting side of the junction, we have

$$\psi_S\left(\mathbf{r}\right) = \psi_S\left(x\right) e^{i(k_y y + k_z z)}. \tag{4.36}$$

The coefficients in Eqs. (4.32) and (4.33) can be determined using the boundary conditions at the interface:

$$\begin{aligned} \psi_N^{\sigma}(0) &= \psi_S(0) \\ \partial_x\psi_S|_{x=0} &- \partial_x\psi_N^{\sigma}|_{x=0} = \mathcal{T}\,\psi_S(0), \end{aligned} \tag{4.37}$$

where

$$\begin{aligned} \mathcal{T} &= k_F Z_0 \hat{\mathbb{I}}_{4\times4} - Z_{soc}\left[k_y \begin{pmatrix} \hat{\sigma}_z & 0 \\ 0 & -\hat{\sigma}_z \end{pmatrix} - k_z \begin{pmatrix} \hat{\sigma}_y & 0 \\ 0 & \hat{\sigma}_y \end{pmatrix}\right] \\ &+ Z_t \begin{pmatrix} 0 & i\hat{\sigma}_x\hat{\sigma}_y\,(k_y + ik_z) \\ -i\hat{\sigma}_y\hat{\sigma}_x\,(k_y - ik_z) & 0 \end{pmatrix}, \end{aligned} \tag{4.38}$$

with the dimensionless parameters $Z_0 = 2mU_0/(\hbar^2 k_F)$, $Z_{soc} = 2mU_{soc}/(\hbar^2 k_F)$ and $Z_t = 2mU_t/(\hbar^2 k_F)$ describing the magnitude of the interfacial usual BTK, the RSOC and the triplet pairing strength. In the analysis of the spin current limit ourselves to the two-dimensional case and in absence of interfacial triplet pairing, namely $Z_t = 0$.

4.6 Spin current

We assume that the quantization axis of the spin is parallel to the $\hat{\boldsymbol{z}}-$direction. From Eq. (4.22) we calculate x- and y-components which correspond, respectively, to perpendicular and parallel component to the interface of the spin current:

$$J_{x,y} = \frac{\hbar}{2m}\int_{-\pi/2}^{\pi/2} d\theta\, Im\left\{\psi^{\dagger}(\mathbf{r}) \begin{pmatrix} \partial_{x,y}\sigma^z & 0 \\ 0 & -\partial_{x,y}\sigma^z \end{pmatrix} \psi(\mathbf{r})\right\}, \tag{4.39}$$

where the integration is extended only over θ, that is the angle formed by the momentum of the electrons propagating from the N side with respect to the normal interface. Inserting the wave functions $\psi_N(\mathbf{r})$ (Eq. (4.35)) and $\psi_S(\mathbf{r})$ (Eq. (4.36) into Eq. (4.39), we have under the Andreev approximation in the normal side:

$$J_x^N = J_0\int_{-\pi/2}^{\pi/2} d\theta\cos\theta\sum_{\sigma}\left[\left(|r_e^{\sigma,\uparrow}(\theta)|^2 - |r_e^{\sigma,\downarrow}(\theta)|^2 + |r_h^{\sigma,\uparrow}(\theta)|^2 - |r_h^{\sigma,\downarrow}(\theta)|^2\right)\right] \tag{4.40a}$$

$$\begin{aligned} J_y^N &= J_0\int_{-\pi/2}^{\pi/2} d\theta\sin\theta\sum_{\sigma} Re\left[\left(|r_e^{\sigma,\uparrow}(\theta)|^2 - |r_e^{\sigma,\downarrow}(\theta)|^2 + |r_h^{\sigma,\uparrow}(\theta)|^2 - |r_h^{\sigma,\downarrow}(\theta)|^2\right.\right. \\ &+ \left.\left. e^{-2ik_F\cos\theta x}\sigma r_e^{\sigma,\sigma}(\theta)\right)\right], \end{aligned} \tag{4.40b}$$

while in the superconducting side of the junction:

$$J_x^S = J_0 \int_{-\pi/2}^{\pi/2} d\theta \cos\theta \sum_\sigma \Big[\left(|u|^2 - |v|^2\right) \Big(|t_e^{\sigma,\uparrow}(\theta)|^2 - |t_e^{\sigma,\downarrow}(\theta)|^2 + |t_h^{\sigma,\uparrow}(\theta)|^2 - |t_h^{\sigma,\downarrow}(\theta)|^2 \Big) \Big] \tag{4.41a}$$

$$J_y^S = J_0 \int_{-\pi/2}^{\pi/2} d\theta \sin\theta \sum_\sigma Re \Big[\left(|u|^2 - |v|^2\right) \Big(|t_e^{\sigma,\uparrow}(\theta)|^2 - |t_e^{\sigma,\downarrow}(\theta)|^2 + |t_h^{\sigma,\uparrow}(\theta)|^2 - |t_h^{\sigma,\downarrow}(\theta)|^2 \Big) + (vu^* - uv^*)\, e^{-2ik_F \cos\theta x} \Big(-t_h^{\sigma,\uparrow}(\theta)\, t_e^{\sigma,\downarrow *}(\theta) + t_h^{\sigma,\downarrow}(\theta)\, t_e^{\sigma,\uparrow *}(\theta) \Big) \Big] \tag{4.41b}$$

where σ corresponds to the spin of the incident electron and $J_0 = \mathcal{N}\hbar k_F/2\pi m$, with $\mathcal{N}/\pi$ related to the number of transverse modes. The expressions in Eqs. (4.40a) and (4.41a) vanish identically when the following conditions are satisfied:

$$\begin{aligned} r_\alpha^{\sigma,\uparrow}(\theta) &= r_\alpha^{\bar\sigma,\downarrow}(-\theta) \\ t_\alpha^{\sigma,\uparrow}(\theta) &= \gamma_\alpha t_\alpha^{\bar\sigma,\downarrow}(-\theta), \end{aligned} \tag{4.42}$$

while those in Eqs. (4.40b) and (4.41b) if:

$$\begin{aligned} r_\alpha^{\sigma,\uparrow}(\theta) &= r_\alpha^{\bar\sigma,\downarrow}(\theta) \\ t_\alpha^{\sigma,\uparrow}(\theta) &= \gamma_\alpha t_\alpha^{\bar\sigma,\downarrow}(\theta), \end{aligned} \tag{4.43}$$

where $\alpha = \{e, h\}$ is the particle index, $\gamma_e = -\gamma_h = 1$, $\sigma = \{\uparrow, \downarrow\}$ and $\bar\sigma = -\sigma$ indicates the spin polarization opposite to σ. From the analytic expression of the scattering coefficients, obtained by applying the boundary conditions at the interface Eqs. (4.37) with $Z_t = 0$, $r_h^{\sigma,\bar\sigma} = \sigma 4uv/\mathcal{A}$, $r_e^{\sigma,\sigma} = -Z\left(u^2 - v^2\right)(2i + Z)/\mathcal{A}$, $t_e^{\sigma,\sigma} = 2u\,(2 - iZ)/\mathcal{A}$ and $t_h^{\sigma,\bar\sigma} = \sigma 2ivZ/\mathcal{A}$, with $\mathcal{A} = 4u^2 + (u^2 - v^2)Z^2$ and $Z = Z_0/\cos\theta - \sigma Z_{soc}\tan\theta$, we can see that Eq. (4.42) is satisfied, from which follows that $J_x^{N/S} = 0$. However, Eq. (4.43) is not satisfied and hence we have $J_y^{N/S} \neq 0$. Thus, in presence of interfacial RSOC we have a transerve spin current whereas there is no spin current flow across the barrier. Now, we want to see if there is indeed a finite value of the tranverse spin current in the N and S sides of the junction. In Fig. 4.1 we plot the transverse spin current J_y/J_0 *vs* $k_F x$ (distance from the interface) at Fermi energy, for $E/\Delta = 10^{-4}$ and $E/\Delta = 0.99$ for different values of Z_0 and Z_{soc} and for $Z_t = 0$, computed by using Eqs. (4.40b) and (4.41b). Two cases

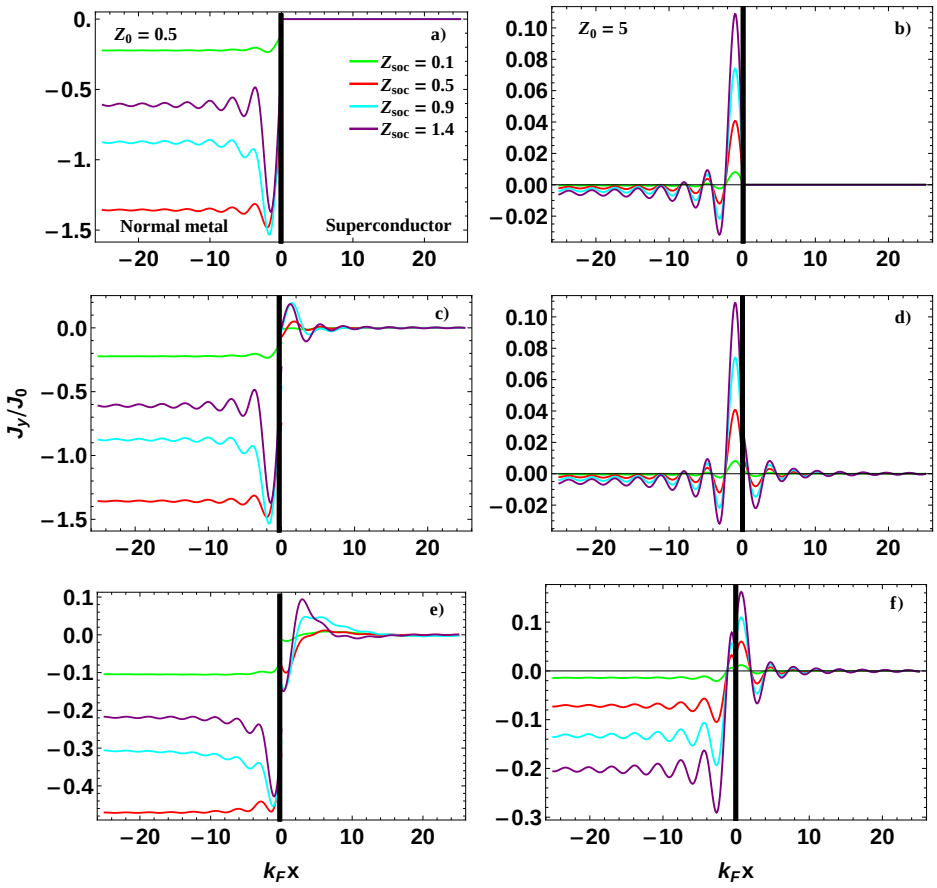

Figure 4.1: Plot of transverse spin current J_y/J_0 *vs* $k_F x$ to vary of Z_1 (values in the panels), for $Z_0 = 0.5$ (left panel) and $Z_0 = 5$ (right panel) at Fermi energy a) and b)), $E/\Delta = 10^{-4}$ c) and d)) and $E/\Delta = 0.99$ e) and f)).

are considered: (*i*) $Z_0 = 0.5$, shown in the left panels; (*ii*) $Z_0 = 5$, shown in the right panels. In each plot, different curves correspond to different values of Z_{soc} (ranging from 0 to 1.4). For $Z_0 = 0.5$ at Fermi energy the spin current persists only in the N region and sature at a constant value (Fig. 4.1 a)). Fixing $E/\Delta = 10^{-4}$ (Fig. 4.1 c)), we observe that near the interface the spin current in superconducting region is different from zero and increases to enhance of Z_{soc}; while in the normal region we have the same behavior than at Fermi energy. This trend persists for $E/\Delta = 0.99$ (Fig. 4.1 e)), where J_y/J_0 in the N region and near the interface in S region increases due to the Andreev reflection. A different scenario is observed for $Z_0 = 5$: the spin current decreases due to a suppression of the Andreev reflection and decays to zero in both the regions at Fermi energy (Fig. 4.1 b)) and for $E/\Delta = 10^{-4}$

(Fig. 4.1 c)), while at the interface assumes the same value in the N region and is different from zero in S region. For $E/\Delta = 0.99$ (Fig. 4.1 f)) note that at the interface J_y/J_0 in the S region is greater than in the N region. Furthermore, in all panels, the spin current presents a discontinuity at the interface ($x = 0$), that is given by the spin torque and can be evaluated via Eq. (4.27). Numerical calculations show that the value of the spin torque at the interface is equal to the discontinuity of the spin current at the interface. Our analysis show that there in not a finite value of the spin current in the superconductor bulk, contrary to what was obtained by Linder *et al.*[70] where a finite spin current in the bulk superconductor is achieved for low values of usual BTK and RSOC potential barrier strengths. In our opinion the difference could lie in an insufficient accuracy of the method of calculation used to simulate the model. The inclusion of the interfacial triplet pairing in the expression for the spin current causes an increase in its value at the interface, but does not change the main features discussed above. In the following, in order to evaluate the effects of a RSOC and its interplay with a triplet pairing, we study the spin differential conductance of the N/S junction in three-dimensional case.

4.7 Spin differential conductance

Ordinarily, Andreev reflection with equal spin as the incoming electron is absent in the N/S junction with standard BTK potential barrier at the interface. However, the presence at the interface of RSOC consider the possibility to have a hole with spin σ and an electron with spin $-\sigma$, where $\sigma = \{\uparrow, \downarrow\}$ is the spin of the incident electron. To illustrate that the amplitudes of these coefficients are nonzero, we consider Fig.4.2 where we have plotted the probability associated to the scattering coefficients for several values of incident angles (θ, ϕ) for the case of high interface transparency as function of E/Δ. In each case, several values of the interfacial RSOC Z_{soc} and triplet pairing Z_t strength are considered, as labelled. Fixing $Z_0 = 0.5$, we consider two cases: (i) $(\theta, \phi) = (0, \pi/2)$ shown in the top panels and (ii) $(\theta, \phi) = (\pi/4, \pi/4)$ shown in the bottom panels. For normal incidence $(\theta, \phi) = (0, \pi/2)$ the anomalous Andreev reflection (AAR) is zero for any value of Z_0, Z_{soc} and Z_t, from which the result of BTK model[32] is reproduced (Fig. 4.2 a), b) and c)). For $(\theta, \phi) = (\pi/4, \pi/4)$, in Fig. 4.2 d) we have $Z_{soc} = 0.5$ and not interfacial triplet pairing, from which results that the AAR is not established. Moreover, we have a reduction of the conventional Andreev reflection (CAR), due to the presence of a finite value of Z_{soc} that reduces carrier density of opposite spin band of the incoming electron. In Fig. 4.2 e) the AAR is

different from zero when we have $Z_t = 0.2$ and not interfacial RSOC. When we allow for both RSOC and triplet pairing scattering potentials, it is seen that AAR is present and its magnitude is higher compared to the previous two situations (Fig. 4.2 f)). To investigate how large the magnitude of the

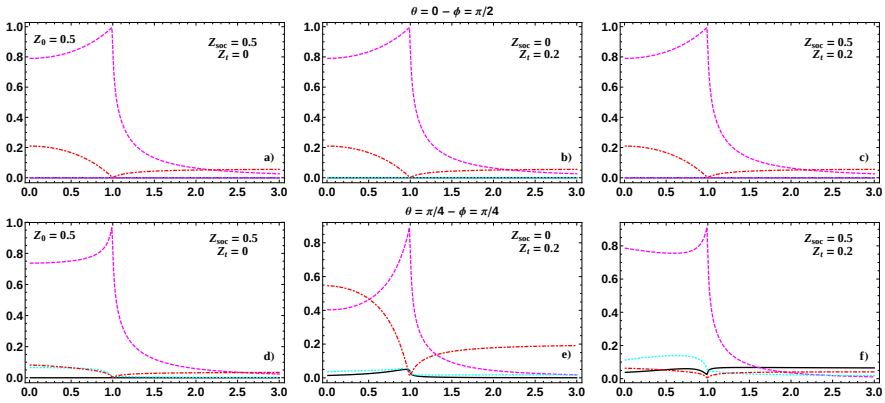

Figure 4.2: Plot of the probability associate with the scattering processes at the interface obtained for different values of (θ, ϕ), Z_{soc}, Z_t and $Z_0 = 0.5$ (values in the panels). For an incident electron with spin σ, the magenta (dashed) line designates Andreev reflection with spin $-\sigma$, the cyan (dotted) line indicates normal reflection with spin σ, the black (full) line corresponds to Andreev reflection with spin σ and the red (dash-dotted) line designates the normal reflection with spin $-\sigma$.

anomalous Andreev reflection coefficient may become, possibly even to the disadvantage of the probabilty associated to the conventional Andreev reflection, we plotted the case $(\theta, \phi) = (\pi/4, \pi/4)$ and $Z_0 = 0.5$ for different values of Z_{soc} and Z_t as shown in Fig. 4.3. It is seen that an increases as Z_{soc} (Fig. 4.3 (top panels) or Z_t (Fig. 4.3 (bottom panels) increase, the probability associated to the AAR grows, but never becomes much larger than the probability for the conventional Andreev reflection. Thus, the presence of a scattering potential that, even if weakly, discriminate between spin-up and spin-down electrons, may induce interesting modifications to the spin transport in N/S junction. In order to capture many essential features of a N/S junction that pertain to both interfacial properties as bulk effects, respectively, on the N and S side, we study the spin conductance. It can be easily obtained from the probability associated with the scattering processes and for each spin channel at $T = 0$, can be written as[32, 88, 89]

$$G_\sigma(E, \theta, \phi) = \sum_{\nu=\uparrow,\downarrow} \left(1 - |r_h^{\sigma,\nu}(E, \theta, \phi)|^2 - |r_e^{\sigma,\nu}(E, \theta, \phi)|^2\right), \tag{4.44}$$

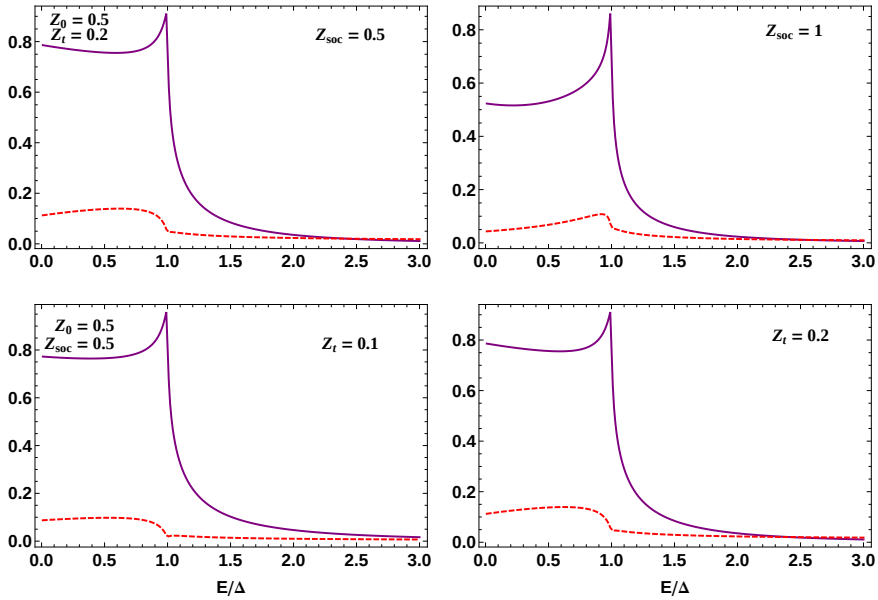

Figure 4.3: Plot of the probability associated to the conventional (purple full line) and anomalous (red dashed line) Andreev reflection for $(\theta, \phi) = (\pi/4, \pi/4)$, $Z_0 = 0.5$ and different values of Z_{soc} and Z_t (values in the panels). It is seen that for increasing of Z_{soc} or Z_t the anomalous Andreev reflction never dominates the conventional Andreev reflection.

where we have used the Andreev approximation and the quantities $\{r_h^{\sigma,\nu}, r_e^{\sigma,\nu}\}$ are the Andreev reflection and normal reflection, respectively. Note that while to the charge current the AR reflected quasiparticles positively contribute, they have negative contribute to the spin current, since their spins are reversed. The total spin conductance is defined as:

$$G_S(V) \propto \sum_{\sigma=\uparrow,\downarrow} \int d^2\boldsymbol{k}_{\parallel} \rho_\sigma G_\sigma(E, \theta, \phi), \tag{4.45}$$

where $\rho_{\uparrow(\downarrow)} = +1\,(-1)$. The above expression can be rewritten in terms of angular integration over the incidence angles (θ, ϕ) fixing the wave vector modulus $k = \sqrt{2mE/\hbar^2}$ and changing the integral variables, i.e. $\int d^2\boldsymbol{k}_{\parallel} = \int k^2 \cos\theta \,(\sin\phi)^2 \, d\theta \, d\phi$. We only consider transport near the Fermi level since our results of spin conductance are obtained as linear response to a small applied bias, thus the wave vector k is well approximated by the constant value k_F and $G_S(V)$ can be rewritten as:

$$G_S(V) \propto \frac{k_F^2 \mathcal{A}}{(2\pi)^2} \sum_{\sigma=\uparrow,\downarrow} \int_0^{\pi} \int_{-\pi/2}^{\pi/2} \mathrm{d}\theta \mathrm{d}\phi \cos\theta \sin^2\phi \rho_\sigma G_\sigma(E, \theta, \phi), \tag{4.46}$$

where $k_F^2\mathcal{A}/(2\pi)^2$ is related to the number of transverse modes which partecipate in the spin transport and the range of integration on the angular variables represent the critical angles for the transmission of electrons with spin σ. To illustrate the effects of the barrier strengths Z_0, Z_{soc} and Z_t we exhibit the spin differential conductance spectra of the N/S junction. Figure 4.4 shows the normalized spin differential conductance G_S/G_N *vs* E/Δ, with $G_N = \sum_{\sigma=\uparrow,\downarrow} G_\sigma\,(E \gg \Delta, \theta, \phi)$, for different values of Z_0, Z_{soc} and Z_t, while Z_0 is fixed as labelled. From Figure 4.4 a), we can see that when $Z_{soc} = 0$,

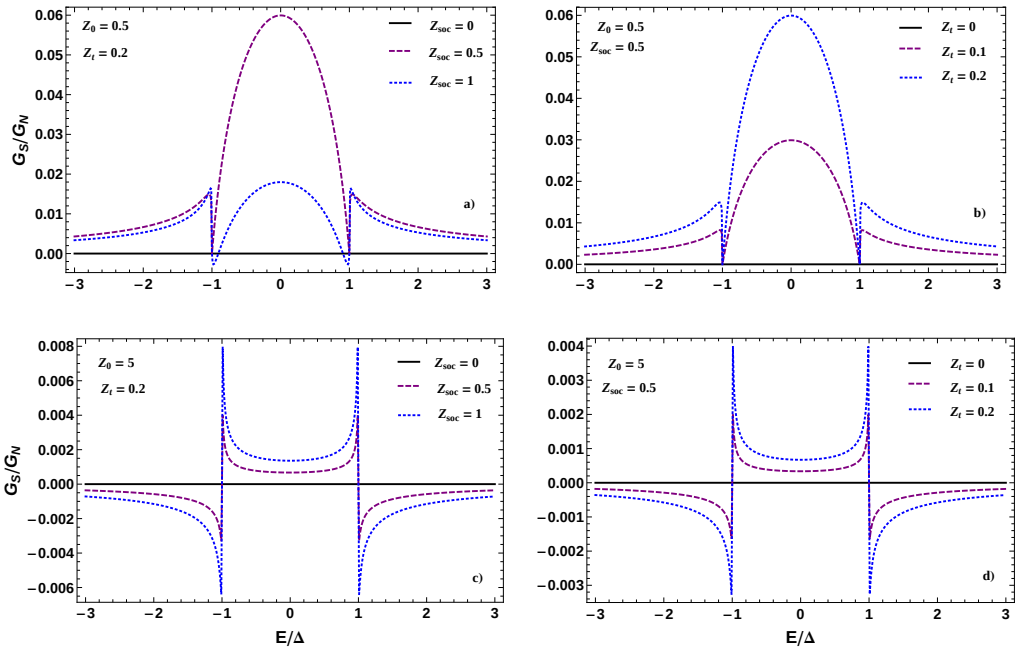

Figure 4.4: Normalized differential conductance curves, G_S/G_N *vs* E/Δ, calculated from Equation (4.46). The different curves are obtained for distinct values of Z_0, Z_1 and Z_t(values in the panels).

G_S/G_N is zero. In this case, the interface RSOC does not induce the Andreev reflection with equal spin as the incoming electron, also if Z_t is different from zero. We can see the same result also for high Z_0 (Fig. 4.4 c)). With increasing Z_{soc} the probability associated to the conventional Andreev reflection decreases, while that of the anomalous Anreev reflection increases and a zero-bias peak forms. The zero-bias peak is higher for small value of the interfacial RSOC strength. When $Z_0 = 5$ (Fig. 4.4 c)) the spin differential conductance quickly decreases and the zero-bias peak disappears, while two peaks at $E/\Delta \approx \pm 1$ appear. It shows that Z_{soc} decreases G_S/G_N when the energy is larger than the gap. Because the contribution of conductance within

the energy gap arises from the Andreev reflection process, the behavior of the spin differential conductance testifies that the Andreev process happens at the circumstances previously described. Fixing $Z_{soc} = 0.5$ (Fig. 4.4 b)), we observe that for $Z_t = 0$ the normalized spin differential conductance is zero. With increasing Z_t, we have the same behavior shown in Fig. 4.4 a), however the zero-bias peak increases since the probability associated to the anomalous Andreev reflection increases. Moreover, G_S/G_N shown in Fig. 4.4 c) is larger than Fig. 4.4 d). It is due to the usual suppression of the Andreev reflection with increasing of the barrier strength. The unusual behavior is that the spin differential conductance always drops at a minimum when the energy E is equal to the energy gap Δ. So the interfacial RSOC can not be viewed as spin-active barrier, but as spin-flip barrier with a dependence on different incident angles[90, 91, 92]. On other hand the enhancement of G_S/G_N with incresing of Z_t plays an important part as spin-active barrier because increases the probabilty to have spin-flip scattering at the interface. We point out that the behavior of the normalized spin differential conductance represents a significant feature on the combined effect of Z_{soc} and Z_t and depends on the actual values of these parameters. In Fig.4.5 we have analyzed the

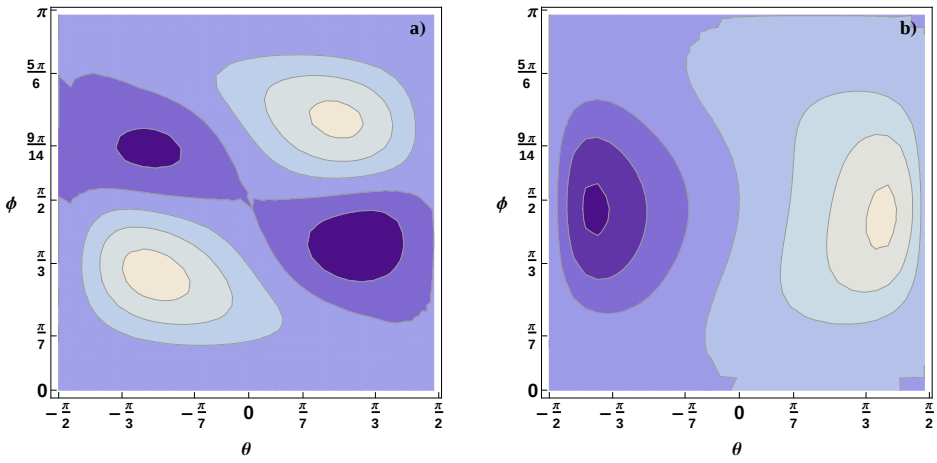

Figure 4.5: Contour plot of the angles-resolved spin conductance. Colors are associated with the values taken by the angles-resolved spin conductance: darker areas indicate lower values. For all the panels, the parameters are fixed as: $Z_0 = 0.5$, $Z_{soc} = 0.5$, $Z_t = 0.2$, a) $E/\Delta = 0.1$ and b) $E/\Delta = 1.5$.

angles-resolved spin conductance $\sum_\sigma \rho_\sigma G_\sigma (E, \theta, \phi) \cos\theta \sin^2\phi$[93] profile for the case of high interface transparency ($Z_0 = 0.5$) to illustrate its behavior as a function of incidence angles (θ, ϕ) and E/Δ for $Z_{soc} = 0.5$ and $Z_t = 0.2$.

For $E/\Delta = 0.1$ the spin conductance exhibits peaks at $(\theta, \phi) \approx (\pm\pi/4, 2\pi/7)$ (Fig. 4.5 a)). For $E/\Delta = 1.5$, instead, the angles-resolved spin conductance shows only one peak at $(\theta, \phi) \approx (2\pi/5, 2\pi/9)$. We have verified that by changing the sign of E/Δ, the angles-resolved spin conductance does not change sign and for low value of interface transparency the angles-resolved spin conductance does not show peaks. Furthermore, for $\phi = \pi/2$, we have $G_\sigma(E, \theta)) = -G_\sigma(E, -\theta)$ for both values of E/Δ, then we integrate over θ $G_S/G_N = 0$[94].
In summary we have demonstrated that in presence of interfacial RSOC there is not present a spin current in the bulk superconductor, but only near the interface. Moreover, take into account the possibility that RSOC at the interface can induce a spin triplet pairing in the superconductor, we have included also an interfacial triplet pairing and we have analyzed the effect of both on the spin conductance. Our results show that to have a spin conductance we must have a triplet pairing at the interface that supports an anomalous Andreev reflection. Such an effect could be useful for spintronics application as magnetic memories and required further theoretical and experimental analysis.

Conclusions

In this work we have investigated the charge and spin transport in normal-metal/superconductor (N/S) junctions with the purpose to describing the interface effects in them. We have considered conventional $s-$wave order parameter symmetry in S. In chapter 3 of this work the analysis has been performed through a generalization of the Blonder-Tinkham and Klapwijk (BTK) theory, by introducing particle-hole mixing boundary conditions in the scattering problem, which are mathematically allowed in the BdG formalism and whose physical meaning can be understood in terms of proximity effect, and solving the corresponding BdG equations. By applying the boundary conditions to the solutions of BdG equations in the normal and superconductive regions, we were able to calculate the probability amplitudes associated to reflection and transmission coefficients and therefore the differential conductance. Our results show the presence of a zero-bias peak surrounded by two dips in the differential conductance spectra, which are not described by the standard BTK model, and which resembles the experimental differential conductance of Cu/Nb junctions obtained by PCAR measurement. The peak-dips structure is obtained when the phase of the particle-hole potential assumes the π value. This value for the phase can be explained in terms of a phase $\pi-$shift between the bulk and the interface parameter order, whose origin can be associated to the presence of localized magnetic moment at the interface. If the magnetic moment at the interface is sufficiently strong, the interfacial phase can assume the π value and there can be a sign change of the superconducting parameter order. We have shown by employing a tight-binding model for the N/S junction with a local magnetic moment at the interface, by calculating self-consistently the gap and the polarization, that the physical conditions under which the $\pi-$shift is realized are related a transparent interfaces that allows to maintain a phase gradient as the effect of a weak interface magnetization. On the other hand for reduced transparencies a larger magnetic moment is necessary to induce the inversion of the interface parameter order. Finally, we have studied the physical meaning of the strength of the parameter that describe the particle-

hole potential by comparing the differential conductance of the generalized BTK with that of a normal-metal/superconductor′/superconductor (N/S′/S) junction, where S is the bulk superconductor and S′ is the superconducting proximity region having a thickness of the order of the coherence length of S and a lower order parameter ($\Delta' < \Delta$). The analysis of the differential conductance of the N/S′/S model has revealed several interesting features on the parameter that quantifies the strength of the particle-hole potential (Z_1) under the assumptions of transparency of the N/S′ interface and low-transparency of the S/S′ interface. Our results suggest that the role of this parameter in the generalized BTK model is similar to that of the ratio of the two order parameters (Δ'/Δ) in the N/S′/S model, confirmed by the presence of peak-dips structure in the conductance of this model. Moreover the presence of this structure in the differential conductance underlines that the parameter Z_1 not only contains information on the proximity effect, but especially is not artifact of the delta-like form of the particle-hole mixing potential. Finally, we have compared the temperature evolution of the conductance spectra obtained in our model with the one calculated by using the reflection and transmission coefficients of the proximity model noting the differences between them. In chapter 4 of this work, as far as the spin transport is concerned, we have considered the effect of a Rashba spin-orbit coupling (RSOC) at the interface an we have studied the spin current and the spin differential conductance. The choice of RSOC is motivated not only by the fact that in hybrid structures the breaking reflection symmetry near the interface gives rise a RSOC that allows spin-flip of the incoming electrons, but also by evidence that materials with a high atomic number show a spin-orbit coupling. The analysis has been performed through an extended BTK approach to include interfacial RSOC and solving the corresponding BdG equations. We have evaluated the spin current and a special emphasis has been devoted to understand its dependence on the strength of the usual BTK barrier potential and RSOC contribution. Our results show that the spin current can flow parallel to the interface, while along the transport direction, in the superconductor, where the influence of RSOC disappears, it goes rapidly to zero. This behavior is in agreement with the fact that in the bulk the order parameter of the superconductor has a singlet component only which prevents a polarized transport. On the other hand, near the interface, RSOC changes the superconductivity character giving rise to a triplet component of the order parameter and then we have both the singlet and triplet components. The main difference between these components is that the singlet component is the source for the triplet one. This triplet component of the order parameter is sustained by the Andreev reflection with equal spin (anomalous Andreev reflection) as the incoming electron. In order to

evaluate the effect of the triplet component in the spin transport of the N/S junction, we have modelled the interfacial potential barrier with RSOC and triplet pairing contributions and we have analyzed the behavior of the spin differential conductance. Our results show that the interfacial RSOC does not provide the spin-flip mechanism which allows the anomalous Andreev reflection to occur. This mechanism must be accompained by the presence of an interfacial triplet pairing, that allows a value different from zero for the spin differential conductance. Our results represent an important tool for the comprehension of the relevant mechanisms that can take place at the interface in superconducting junctions. They can also be useful in spintronics applications to detect and control the spin transport.

Bibliography

[1] P. G. de Gennes, Rev. Mod. Phys. **36**, 225 (1964).

[2] N. M. Werthamer, Phys. Rev. **132**, 2440 (1963).

[3] P. C. van Son, H. van Kempen and P. Wyder, Phys. Rev. Lett. **59**, 2226 (1987).

[4] Y. de Wilde, J. Heil, A. G. M. Jansen, P. Wyder, R. Deltour, W. Assmus, A. Menovsky, W. Sun and L. Taillefer, Phys. Rev. Lett. **72**, 2278 (1994).

[5] Ch. Walti, H. R. Ott, Z. Fisk and J. L. Smith, Phys. Rev. Lett. **84**, 5616 (2000).

[6] K. Gloos, Phys. Rev. Lett. **85**, 5257 (2000).

[7] S. Datta, *Electronic Transport in Mesoscopic Systems*, Cambridge University Press, 1995.

[8] K. Hirose and N. Rabayashi, *Quantum Transport Calculations for Nanosystems*, CRC Press, New York, 2014.

[9] T. Ihn, *Semiconductor Nanostructures*, Oxford University Press, 2010.

[10] T. Ouisse, *Electron Transport in Nanostructures and Mesoscopic Devices*, John Wiley & Sons, London, 2008.

[11] D. K. Ferry, S. M. Goodnick and J. Bird, *Transport in Nanostrustures*, Cambridge University Press, New York, 2009.

[12] H. Fröhlich, Phys. Rev. **79**, 845 (1950).

[13] L. N. Cooper, Phys. Rev. **104**, 1189 (1956).

[14] J. Bardeen, L. N. Cooper and J. R. Schrieffer, Phys. Rev. **106**, 162 (1957); J. Bardeen, L. N. Cooper and J. R. Schrieffer, Phys. Rev. **108**, 1175 (1958).

[15] G. Grosso and G. Pastori Parravicini, *Solid State Physics*, Academic Press, New York, 2003.

[16] G. F. Bassani and U. M. Grassano, *Fisica dello Stato Solido*, Bollati Boringhieri, 2000.

[17] P. J. Ford and G. A. Saunders, *The Rise of Superconductors*, CRC Press, London, 2005.

[18] R. Meservey and B: B. Schwartz, *Equilibrium properties: Comparison of Experimental Results with Predictions of BCS Theory*, R. D. Parks, New York, 1969.

[19] P. G. de Gennes, *Superconductivity of Metals and Alloys*, W. A. Benjamin, New York, 1966.

[20] D. Daghero and R. S. Gonnelli, Supercond. Sci. Technol. **23**, 043001 (2001).

[21] R. J. Soulen Jr, J. M. Byers, M. S. Osofsky, B. Nadgorny, T. Ambrose, S.F. Cheng, P.R. Broussard, C.T. Tanaka, J. Nowak, J. S. Moodera, A. Barry, J. M. D. Coey, Science **282**, 85 (1998).

[22] S. K. Upadhyay, A. Palanisami, R. N. Louie and R.A. Buhrman, Phys. Rev. Lett. **81**, 3247 (1998).

[23] A. F. Andreev, Sov. Phys. JETP **51**, 111 (1980) [Zh. Eksp. Teor. Fis. **46**, 1823 (1964)].

[24] B. Pannetier e H. Courtois J. Low Temp. Phys. **118**, 599 (2000).

[25] G. Deutscher and P. de Gennes, *Superconductivity*, Dekker, New York, 1969.

[26] T. M. Klapwijk, J. Supercond. Nov. Magn. **17**, 593 (2004).

[27] M. Tinkham, *Introduction To Superconductivity*, McGraw-Hill, New York, 1996.

[28] G. Deutscher, Rev. of Mod. Phys., **77**, 109 (2005).

[29] J. F. Annett, *Superconductivity, Superfluids, and Condensates*, Oxford University Press, New York, 2004.

[30] M. J. M. de Jong and C. W. J. Beenakker, Phys. Rev. Lett. **64**, 1657 (1995).

[31] I. I. Mazin, A. A. Golubov and B. Nadgorny, J. Appl. Phys., **89**, 7576 (2001).

[32] G. E. Blonder, M. Tinkham and T. M. Klapwijk, Phys. Rev. B **25**, 4515 (1982).

[33] G. J. Strijkers, Y. Ji, Y. Yang, C. L. Chien and J. M. Byers, Phys. Rev. B **63**, 104510 (2001).

[34] L. Shan, H. Tao, Z. Li, Z. A. Ren G. C. Che and H. H. Wen, Phys. Rev. B **68**, 1445510 (2003).

[35] G. Sheet, S. Mukhopadhyay and P. Raychaudhuri, Phys. Rev. B **69**, 134507 (2004).

[36] C. Rossetti, *Istituzioni di Fisica Teorica*, Levrotto & Bella, Torino, 1990.

[37] G. T. Woods, R. J. Soulen, I. Mazin, B. Nadgorny, M. S. Osofsky,J. Sanders, H. Srikanth, W. F. Egelhoff and R. Datla, Phys. Rev. B **70**, 054416 (2004).

[38] Y. Tanaka, A. A. Golubov and S. Kashiwaya, Phys. Rev. B **68**, 054513 (2003).

[39] S. Kashiwaya, Y. Tanaka, M. Koyanagi and K. Kajimura, Phys. Rev. B **53**, 2667 (1996).

[40] I. Žutić and O. T. Valls, Phys. Rev. B **61**, 1555 (2000).

[41] N. L. Bobrov, S. I. Beloborodko, L. V. Tyutrina, I. K. Yanson, D. G. Naugle and K. D. D. Rathnayaka, Phys. Rev. B **71**, 014512 (2005).

[42] A. Pleceník, M. Grajcar, Š. Beňačka, P. Seidel and A. Pfuch, Phys. Rev. B **49**, 10016 (1994).

[43] H. Srikanth and A. K. Raychaudhuri, Physica C **190**, 229 (1992).

[44] Y. de Wilde, T. M. Klapwijk, A. G. M. Jansen, J. Heil and P. Wyder, Physica B **218**, 165 (1996).

[45] Y. Miyoshi, Y. Bugoslavsky and L. F. Cohen, Phys. Rev. B **72**, 012502 (2005).

[46] C. L. Chien and D. H. Reich,J. Magn. Magn. Mater. **200**, 83 (1999).

[47] M. Catapano, F. Romeo, R. Citro and F. Giubileo, Eur. Phys. J. B **88**, 329 (2015).

[48] F. Giubileo, F. Romeo, R. Citro, A. Di Bartolomeo, C. Attanasio, C. Cirillo, A. Polcari and P. Romano, Physica C **503**, 158 (2014).

[49] H. Srikanth and A. K. Raychaudhuri, Phys. Rev. B **46**, 14713 (1992).

[50] Li Zhang-Zhi, Tao Hong-Jie, Xuan Yi, Ren Zhi-An, Che Guang-Can and Zhao Bai-Ru, Phys. Rev. B **66**, 064513 (2002).

[51] P. Xiong, G. Xiao and R. B. Laibowitz, Phys. Rev. Lett. **71**, 1907 (1993).

[52] A. Barone and G. Paternò, *Physics and Applications of the Josephson effect*, (John Wiley & Sons, New York, 1982).

[53] C. B. Azzoni, A. Paleari and G. B. Parravicini, J. Condens. Matter **4**, 1359 (1992).

[54] T. Kontos, M. Aprili, J. Lesueur and X. Grison, Phys. Rev. Lett. **86**, 304 (2001).

[55] F. Giubileo, F. Romeo, R. Citro, A. Di Bartolomeo, C. Attanasio, C. Cirillo, A. Polcari, P. Romano arXiv:1407.4906.

[56] F. S. Bergeret, A. Levy Yeyati and A. Martín-Rodero, Phys. Rev. B **72**, 064524 (2005).

[57] J. A. Appelbaum, Phys. Rev. B **154**, 633 (1967).

[58] M. N. Baibich, J. M. Broto, A. Fert, F. Nguyen Van Dau, F. Petroff, P. Etienne, G. Creuzet, A. Friederich and J. Chazelas, Phys. Rev. Lett. **61**, 2472 (1988).

[59] G. Binash, P. Grünberg, F. Saurenbach and W. Zinn, Phys. Rev. B **39**, 4828 (1989).

[60] M. M. Glazov, E. Ya. Sherman and V. K. Dugaev, Physica E **42**, 2157 (2010).

[61] T. P. Pareek and P. Bruno, Pramana **58**, 293 (2002).

[62] E. I. Rashba, Fiz. Tverd. Tela **2**, 1224 (1960)[Sov. Phys. Solid State **2**, 1109 (1960)].

[63] Yu. A. Bychov and E. I. Rashba, Pris'ma Zh. Eksp. Teor. Fiz. **39**, 66 (1984)[JETP Lett. **39**, 78 (1984)].

[64] G. Engels, J. Lange Th. Schäpers and H. Lüth, Phys. Rev. B **55**, R1958 (1997).

[65] I. Zütic, J. Fabian and S. D. Sarma, Rev. Mod. Phys. **76**, 323 (2004).

[66] T. Yokoyama, Y. Tanaka and J. Inoue, Phys. Rev. B **74**, 035318 (2006).

[67] Y. Mizuno, T. Yokoyama and Y. Tanaka, Phys. Rev. B **80**, 195307 (2009).

[68] S. Wu and K. V. Samokhin, Phys. Rev. B **81**, 214506 (2010).

[69] S. Wu and K. V. Samokhin, Phys. Rev. B **82**, 184501 (2010).

[70] J. Linder and T. Yokoyama, Phys. Rev. Lett. **106**, 237201 (2011).

[71] F. S. Bergeret and I. V. Tokatly, Phys. Rev. B **89**, 134517 (2014).

[72] V. M. Edelstein, Phys. Rev. B **67**, 020505 (2003).

[73] M. Duckheim and P. W. Brouwer, Phys. Rev. B **83**, 054513 (2011).

[74] S. Takei and V. Galitski, Phys. Rev. B **86**, 054521 (2012).

[75] J. B. Ketterson and S. N. Song, *Superconductivity*, Cambridge University Press, United Kingdom, 1999.

[76] Q. F. Sun and X. C. Xie, Phys. Rev. B **72**, 245305 (2005).

[77] L. Berger, J. Appl. Phys. **55**, 1954 (1984).

[78] P. P. Freitas and L. Berger , J. Appl. Phys. **57**, 1266 (1985).

[79] F. Romeo and R. Citro, Phys. Rev. B **81**, 045307 (2010).

[80] J. D. Jackson, *Classical Electrodynamics*, John Wiley & Sons, New York, 1998.

[81] H. A. Kramers, Proc. Amsterdam Acad. **33**, 959 (1930).

[82] Zhi Ping Niu, Appl. Phys. Lett. **101**, 062601 (2012).

[83] S. B. Chung, H. J. Zhang, X. L. Qi and S. C. Zhang, Phys. Rev. B **84**, 060510 (2011).

[84] S. Takei, B. M. Fregoso, V. Galitski and S. D. Sarma, Phys. Rev. B **87**, 014504 (2013).

[85] J. P. Heida, B. J. van Wees, J. J. Kuipers, T. M. Klapwijk and G. Borghs, Phys. Rev. B **57**, 11911 (1998).

[86] J. Nitta, T. Akasaki, H. Takayanagi and T. Enoki, Phys. Rev. Lett. **78**, 1335 (1997).

[87] D. Grundler, Phys. Rev. Lett. **84**, 6074 (2000).

[88] S. Kashiwaya, Y. Tanaka, N. Yoshida and M. R. Beasley, Phys. Rev. Lett. **74**, 3451 (1995).

[89] Y. Tanaka, T. Yokoyama and S. Kashiwaya, Phys. Rev. B **79**, 060505(R) (2009).

[90] C. D. Feng, Z. M. Zheng, R. Sheng, B. Wang and D. Y. Xing, Phys. Rev. B **81**, 224510 (2010).

[91] B. Lv, Eur. Phys. J. B **83**, 493 (2011).

[92] Z. P. Niu, EPL **100**, 17012 (2012).

[93] Y. Tanaka, T. Yokoyama, A. V. Balatsky and N. Nagaosa, Phys. Rev. B **79**, 060505(R) (2009).

[94] M. Catapano, F. Romeo and R. Citro, in preparation.